Ten Noorden van de Waddeneilanden Field Measurement Campaign

Validation Report - December 2020

Deltares

Ten Noorden van de Waddeneilanden Field Measurement Campaign

Validation Report - December 2020

Sofia Caires

11203488

Deltares

Title
Ten Noorden van de Waddeneilanden Field Measurement Campaign

Classification
None

Keywords
North Sea, wind farm, metocean data, validation, offshore wind

Summary
Two *SEAWATCH Wind LiDAR Buoys*, TNWA and TNWB, have been deployed by Fugro at the Ten Noorden van de Waddeneilanden Wind Farm Zone on the 19th of June 2019, with the intention of measuring wind, waves, temperatures, pressures and currents for a period of two years. In order to also collect bottom temperature and water level data, two bottom mounted sensors have then also been deployed near TNWA and TNWB. The redundant arrangement of instruments is intended to safeguard against loss in measured data. In order to further avoid gaps in the data, there has been some servicing and swapping of the buoys and sensors when needed.

In this report the validation of the measurements during December 2020 is presented.

A few issues have affected the data availability. Consequently, there is only a handful of wind direction observations available from the LiDAR at TNWA and there are no current data available from TNWB. Furthermore, because the bottom mounted sensors are either not in place or have dropped out, there are no bottom temperature nor water level data available. On the other hand, the availability of wind data from the sensor at TNWA and the LiDAR and sensor at TNWB, of surface water temperature, pressure and waves from both buoys, of air temperature from TNWB and of current data from TNWA is high. The availability of air temperature from TNWA is good and the availability of wind speed data from the LiDAR at TNWA is limited to acceptable. In summary, when considering the redundant arrangement of instruments, nearly all of the expected data are available during this period.

The validation of the available data is performed by intercomparing the TNWA and TNWB observations and validating against wind, waves, air and water temperature, air pressure and currents from a variety of reliable sources (anemometer, LiDAR, hydrodynamic model, etc) at reference stations in the North Sea; namely L91, K13, F3, AWG, HG, SON and BG.

The following conclusions ensue from the validation of the data.

- The comparisons between the TNWA and TNWB wind speeds (there are not enough wind direction data from TNWA for meaningful wind direction comparisons) show at all levels low biases and correlations and slopes close to 1, indicating correct functioning of both LiDARs. Furthermore, there is a reasonable (distant or affected by local features stations) to excellent (nearby stations) agreement between the wind observations from TNW and those from the fixed platforms. The found mismatches can be explained by local effects and spatial and vertical variations.
- The agreement between the TNWA and TNWB wave parameters is excellent for all parameters, except in terms of peak wave period which is reasonable and swell mean wave direction which is poor. The poorer agreements are as expected, given that these parameters depend more strongly on the sampling variability (randomness of the sea surface elevation) and discreteness of the wave spectra. The agreement between the

wave observations from TNW and from the reference stations is relatively high, with the found mismatches being due to local effects, spatial variations and again discreteness of the wave spectra.
- The validation of the temperature data shows that there is an excellent agreement between TNW air temperature observations and those from the considered fixed station. Furthermore, due to spatial variations there are mismatches between TNW surface water temperature observations and those from the fixed stations.
- The validation of the air pressure data shows, as expected given their proximity in terms of macro-atmospheric forcings, an excellent agreement between the TNW observations and those from the fixed stations.
- The agreement between the TNWA current speed observations and model results is high. There are mismatches between the current directions, which are partly due to the nature and variability of the current direction signal.

The overall conclusion of the validation is that the TNW dataset is of high quality and trustworthy.

References
None

Version	Date	Author	Initials	Review	Initials	Approval	Initials
2.0	Mar. 30, 2021	S. Caires		J. Schouten		M. van Gent	

Status
Final

Contents

Deltares

List of Figures

Deltares

List of Tables

Deltares

1 Introduction

Aiming at high collection rates of quality metocean data, two *SEAWATCH Wind LiDAR Buoys* were deployed by Fugro at the Ten Noorden van de Waddeneilanden Wind Farm Zone. The two buoys are referred to as Station A and Station B but are abbreviated in this report as TNWA and TNWB, respectively. Additionally, bottom mounted water level sensors (WLS) have been deployed near the buoys. The deployment date is the 19th of June 2019, when buoy WS190 was deployed at TNWA and buoy WS191 deployed at TNWB. The campaign aims at measuring wind, waves, temperatures, pressures and currents for a period of two years.

The redundant arrangement of instruments is intended to safeguard against loss in measured data. This is an efficient approach given that it has led to an almost continuous data record per variable from TNW in spite of a few problems. Unfortunately, often problems can only be solved by going to the site and servicing or replacing the buoys. In the following the issues and deployment and recovery events that have led to relevant data gaps are listed. The full record of issues is given in the report of Fugro accompanying the data.

- Communication with the WLS at TNWA failed right after deployment in June 2019.
- Connection was lost with the LiDAR at TNWB from the 12th of September 2019 until the 23rd of January 2020, when the buoy was serviced and the data downloaded.
- The LiDARs on both buoys stopped working at the end of December 2019.
- On the 22nd of January 2020 buoy WS190 was swapped with buoy WS170 at TNWA and buoy WS191 at TNWB removed. With no TNWB buoy and WLS data being available from this date. Due to weather constrains it was not possible to deploy a buoy at TNWB until April 2020.
- On the 11th of April buoy WS170 was recovered and buoy WS190 deployed at TNWA and buoy WS191 deployed at TNWB. From this time WLS observations from both TNWA and TNWB are available.
- Because of performance problems with the LiDAR at WS191, on the 24th of June 2020 buoy WS191 was swapped with buoy WS170 at TNWB.
- Again due to LiDAR performance issues, there was a swap of buoy WS190 with buoy WS191 at TNWA (same mooring) on the 22nd of July 2020.
- On the 14th of September 2020 buoy WS170 was swapped with buoy WS190 at TNWB.
- At 11:20 on the 25th of October 2020 buoy WS190 started drifting, with no data being available from TNWB from this date until 07:40 on the 10th of November 2020 when buoy WS156 was deployed at TNWB.
- At 11:30 on the 30th of December 2020 buoy WS191 at TNWA began to drift and data are missing from that point onwards.

Information regarding the approximate location of the buoys during this reporting period is given in Table 1.1. As the WLS have been deployed close to the buoy, its coordinates are assumed to coincide with those of the buoy. The bathymetry around the approximate location of the buoys is shown in Figure 1.1.

Table 1.1: *Ten Noorden van de Waddeneilanden LiDAR Buoy mooring locations and hull numbers (December 2020).*

Station	Hull number	Longitude (E)	Latitude (N)	Depth (mMSL)
TNWA	WS191	5.5502°	54.0181°	≈ 38
TNWB	WS156	5.5498°	54.0218°	≈ 38
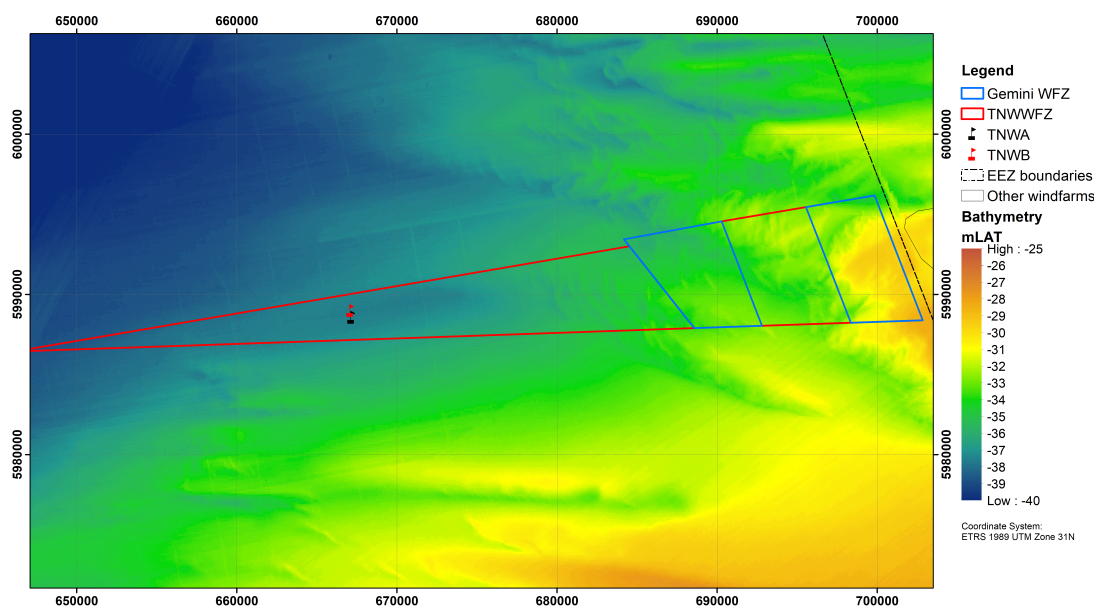
Figure 1.1: *Bathymetry (mLAT, mLAT≈ -1 mMSL) around the buoy locations.*

The main aim of this report is to provide an overview and validation of the TNW post-processed wind, wave, temperature, air pressure, water level and current observations, mainly focusing on the validation of the wind, wave and current data. The assessment of the integrity of the buoy data processing and the quality of the pre-processed data are outside the scope of the validation. The validation is carried out by quantifying the agreement between the TNWA and TNWB data, indicating correct functioning of the different sensors without loss of accuracy, and data from other reliable sources (anemometer, LiDAR, atmospheric model, hydrodynamic model, etc) at fixed North Sea reference stations (no temporary campaigns). If the same variations are found in the parameters, this can be seen as an indication that both buoy systems are functioning correctly with no system errors in the measurements. Furthermore, for some variables their general characteristics are also qualitatively assessed, such as for current and wind measurements their respective vertical profiles. Per variable the most suitable available data validation sources have been sought, leading to the following combinations:

- The reference stations for validating the buoy wind data against anemometer observations are those from platform L91 (where the anemometer is at height z=87 m), referred to as L91, platform K13 (z=73.8 m), referred to as K13, platform Ameland Westgat (z=60 m), referred to as AWG and those from the Huibergat station (z=18 m), referred to as HG. These stations are approximately at a distance of respectively 59 km (L91), 178 km (K13), 64 km (AWG) and 75 km (HG) from the TNW buoys. In previous reports also anemometer observations from F3 (z=60 m, distance=107 km) and F161 (z=75.5 m, distance=101 km) have been used to validate the TNW observation, but there are no valid wind observations from F3 during this period and platform F161 is no longer active (all instruments were removed at the end of August 2020). The considered anemometer observations, as most other observations considered in this study, have been collected by the Dutch Government (see http://matroos.rws.nl/). LiDAR wind velocity observations at vertical levels 63 m, 91 m, 116 m, 141 m, 166 m, 191 m and 241 m at K13 from the Dutch organization for applied research (TNO) have also been made available and are also considered in the validation of the wind data, in particular the variations with height. The validation against the fixed stations observations is complemented using winds at 10 m height from the Dutch Meteorological Institute (KNMI) operational Numerical Weather Prediction model Hirlam7.2 (KNMI, 2009) to evaluate the wind velocity spatial variations during the reporting

period.

- The wave heights, periods and directions are also validated against Dutch Government observations. The locations for validating the buoy wave data are F3 and Schiermonnikoog Noord, referred to as SON and at about 62 km from the TNW buoys.
- The Dutch Government observations at K13 and SON are used for validating the water temperature.
- Available online data (`https://mesonet.agron.iastate.edu/request/download.phtml?network=NL__ASOS`) from weather stations located at Buitengaats, referred to as BG and located within the TNW region, are used for validating the air temperature.
- Dutch Government observations at K13, F3 and L91 are used for validating air pressure.
- Lastly, given the lack of fixed observation sources, the currents are validated against predictions from a purposely run by Deltares 3D hydrodynamic model.

Figure 1.2 shows an overview of all measurement locations. The present report provides the validation results for the period - 'December 2020' - extending from December 01 00:00 to December 31 23:50.

Figure 1.2: *Aerial view of the location of the buoys and fixed measurement stations (via Google Earth).*

All comparisons are presented as a timeseries and further validated via direct scatter plots for quantifying statistical correspondence between the datasets.

The error statistics are computed differently whether a linear or circular (directional) variable is considered. For linear variables we have:

- the bias: $\bar{y} - \bar{x}$;
- the root-mean-square error: rmse = $\sqrt{n^{-1} \sum (y_i - x_i)^2}$;
- the symmetric slope: s = $\sqrt{\sum y_i{}^2 / \sum x_i{}^2}$; and

- the correlation coefficient:

$$r = \sum \left[(x_i - \bar{x})\,(y_i - \bar{y}) \right] / \sqrt{\sum (x_i - \bar{x})^2 \sum (y_i - \bar{y})^2}\ .$$

In all these formulae x_i usually represents observations (or the dataset which is considered less uncertain or baseline) and in this study we use it to represent the fixed observations, y_i usually represents the model results (or the dataset which is considered more uncertain or with a certain deviation from the baseline results) and in this study we use it to represent the TNWA and TNWB data and n the number of observations.

When dealing with circular data, each observation is considered as unit vector, and it requires vector addition rather than ordinary (or scalar) addition to compute the average of angles, the so-called mean direction.

Writing

$$C_n = \sum_{i=1}^{n} \cos x_i \quad and \quad S_n = \sum_{i=1}^{n} \sin x_i, \tag{1.1}$$

the sample resultant vector R_n of a sample $\mathbf{x} = x_i,\ i = 1, ..., n$ is defined as $R_n = \sqrt{C_n^2 + S_n^2}$, and its sample mean direction $\bar{x} \equiv \bar{x}_n$ as the direction of R_n:

$$\bar{x} = TAN^{-1}(S_n/C_n\ )$$

where

$$TAN^{-1}(S_n/C_n\ )$$

is the inverse of the tangent of

$$(S_n/C_n\ )$$

in the range $[0, 2\pi]$, i.e.,

$$TAN^{-1}(S_n/C_n\ ) := \begin{cases} \tan^{-1}(S_n/C_n\ ), & S_n > 0,\ \ C_n > 0 \\ \tan^{-1}(S_n/C_n\ ) + \pi, & C_n < 0 \\ \tan^{-1}(S_n/C_n\ ) + 2\pi, & S_n < 0,\ \ C_n > 0. \end{cases} \tag{1.2}$$

The sample mean resultant length of $\mathbf{x} = x_i,\ i = 1, ..., n$ is defined by $\bar{R}_n = R_n/n$, $0 \leq \bar{R}_n \leq 1$. If $\bar{R}_n = 1$, then all angles coincide.

Equation 1.2 can be used to compute the bias between two circular variables by substituting x_i by $y_i - x_i$ in Equation 1.1. In a similar way, the root-mean-square error between two circular variables can be computed.

There are several circular analogues of the correlation coefficient, but the most widely used is the so-called T-linear correlation coefficient (Fisher and Lee (1983) and Fisher (1993)). Given two sets $\mathbf{x} = x_i,\ i = 1, ..., n,\ \mathbf{y} = y_i,\ i = 1, ..., n$ of circular data, the T-linear correlation coefficient between x and y is defined by

$$r = \frac{\displaystyle\sum_{1 \leq i < j \leq n} \sin(x_i - x_j)\sin(y_i - y_j)}{\sqrt{\displaystyle\sum_{1 \leq i < j \leq n} \sin^2(x_i - x_j) \sum_{1 \leq i < j \leq n} \sin^2(y_i - y_j)}}. \tag{1.3}$$

In the following we shall refer to comparisons in which r is higher than 0.9 as excellent, between 0.8 and 0.9 as good, between 0.7 and 0.8 as reasonable and lower than 0.7 as poor. Note that this is no absolute quality statement given that there are uncertainties in both observations and, due to the distance between the instruments, the spatial variability is expected to affect the comparisons.

Note that all reported dates are in GMT (which is equivalent to UTC).

1.1 Outline of the report

The availability of the considered TNW data is given in the next chapter, followed by the description and validation of the wind, wave, temperature, pressure and current data in separate chapters. A summary of the drawn conclusions is given in the executive summary at the start of this report.

2 Data Availability

Although in measuring campaigns the aim is always of having a full (gap free) timeseries of all measured parameters, they are typically hampered by severe metocean conditions and loss of signal between instruments. Figure 2.1 shows a detailed breakdown for each buoy of the amount of missing data throughout the temporal record for each measured parameter. The availability of the data is computed from December 01 00:00 to December 31 23:50. Note that in this validation study only processed data (10 minute averages in the case of wind) are considered. The original raw observations have been processed and quality checked by Fugro. Furthermore, data from all processed variables are supposed to be available every 10 minutes (at the hour and 10, 20 30, 40 and 50 minutes after the hour). Table 2.1 gives a brief explanation of what the variable names in Figure 2.1 mean, their units and, if applicable, the symbols used to refer to them.

As can be seen in Figure 2.1, the collected data consists of wind speed and direction at different heights, a number of wave height, period and direction parameters, current speed and direction at different depths, water and air temperature, pressure and humidity.

We use the following qualification of data availability:

- >95% referred to as high availability,
- 90 - 95% referred to as good availability,
- 80 - 90% referred to as acceptable availability,
- 60 - 80% referred to as limited availability, and
- <60% referred to as poor availability.

A few issues have affected the data availability:

- There is only a handful of wind direction observations from the LiDAR at TNWA and there are no current data available from TNWB.
- There are no bottom temperature nor water level data available because there is no WLS at TNWB and the one at TNWA dropped out at the start of October 2020.
- From 11:30 on the 30th of December 2020 no data are available from TNWA, because the buoy then started to drift.

On the other hand, the availability of wind data from the Gill sensor at TNWA and the LiDAR and Gill sensor at TNWB, of surface water temperature, pressure and waves from both buoys, of air temperature from TNWB and of current data from TNWA is high. The availability of air temperature from TNWA is good and the availability of wind speed data from the LiDAR at TNWA is limited to acceptable.

Not all data being measured are considered in this report:

- Although the availability of the humidity data is given in Figure 2.1, the data are not considered further.
- The buoys are also recording the wave spectra, but they are not transmitted on an ongoing basis and therefore also not considered on a monthly basis.
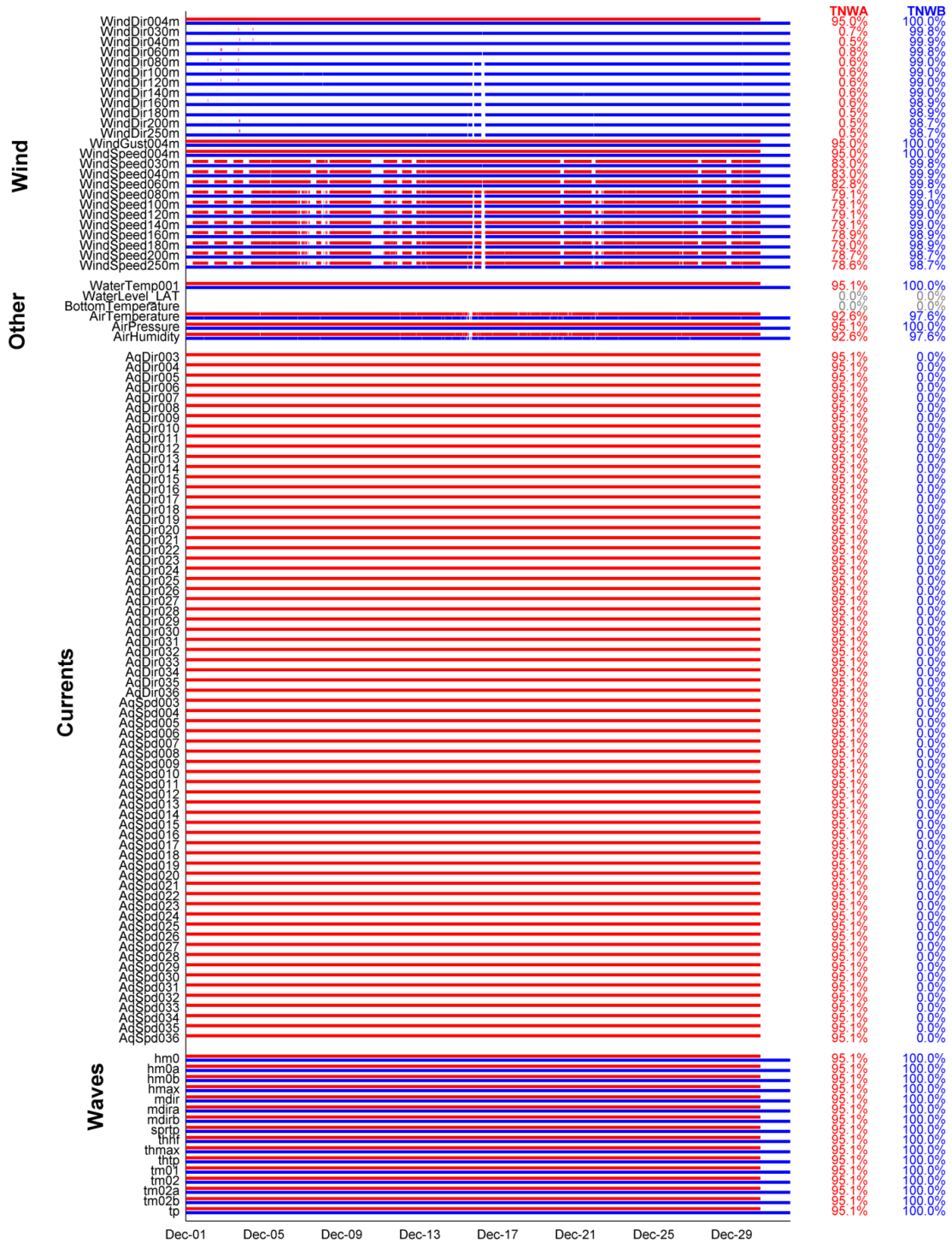
Figure 2.1: *Availability of the 10 minute TNWA (red), TNWB (blue) and WLS (grey) data of December 2020.*

Deltares

Table 2.1: List of variables.

Name	Description	Units	Symbol
WindSpeed z mh	Wind speed at an elevation of z m above the sea surface	m/s	U_z
WindGust z mh	Wind gust speed at an elevation of z m above the sea surface	m/s	
WindDir z m	Wind direction at an elevation of z m above the sea surface	°N	$U_{z\theta}$
airTemperature	Air temperature	°C	T_{air}
airPressure	Air pressure	hPa	
airHumidity	Air humidity	%	
WaterTemp001	Water temperature (surface)	°C	T_{water}
WaterLevel	Still water level	m LAT	WL
BottomTemp	Water temperature (bottom)	°C	T_{water}
AqSpd d	Current speed at a depth of d m below the sea surface	m/s	u_d
AqDir d	Current direction at a depth of d m below the sea surface	°N	
hm0	Spectral significant wave height	m	H_s
hm0a	Spectral significant swell wave height. Frequency band between 0.04 and 0.10 Hz.	m	H_{sswell}
hm0b	Spectral significant sea wave height. Frequency band between 0.10 and 0.50 Hz.	m	H_{ssea}
hmax	Spectral maximal individual wave height	m	H_{max}
mdir	Mean wave direction	°N	MWD
mdira	Mean wave direction of swell	°N	MWD_{swell}
mdirb	Mean wave direction of sea	°N	MWD_{sea}
sprtp	Wave spreading at spectral peak period	°	$DSPR$
thhf	High frequency mean wave direction. Frequency band between 0.4 and 0.44 Hz.	°N	
thmax	Period of highest wave.	s	$T_{H_{max}}$
thtp	Wave direction at spectral peak period.	°N	
tm0x	Spectral mean absolute wave period (1 based on the 1st spectral moment, 2 based on the 2nd spectral moment, a swell, b sea)	s	T_{m0x}
tp	Spectral peak wave period	s	T_p

3 Wind

This chapter focuses on the validation of the wind velocity observations from the *SEAWATCH LiDAR Buoys*. The wind speed and direction are measured at 4 m above water level by a Sonic wind sensor and at levels 30, 40, 60, 80, 100, 120, 140, 160, 180, 200 and 250 m above water level by a LiDAR.

An overview and intercomparison of the TNW wind data is given next, followed by a validation using observed and model data.

Given that for low wind speeds there is much scatter in the data and that these data are not relevant in the data analyses (profiles and error statistics), all observations for which the observed wind speeds are below 5 m/s are excluded. This threshold was chosen pragmatically, being in line with the work of Wieringa and Rijkoort (1983) and in line with other wind climate assessments of the Dutch meteorological institute and close to the 4 m/s threshold prescribed for the calibration of cup anemometers in the IEC 61400-12-1 standard.

3.1 Ten Noorden van de Waddeneilanden description and intercomparison

During this period there is only a handful of wind direction observations from TNWA. For completeness, these data are given in the plots and used in the computation of statistics, but the data and resulting statistics are due to the very small sample size not commented upon.

To get a full overview of the data two movies are created with the time evolution of vertical wind profiles at TNWA (see here) and at TNWB (see here).

Figure 3.1 provides an overview of the observed LiDAR data without the filtered low observations. The figure shows all observed vertical profiles for which the wind speed is above 5 m/s (grey lines), the mean profile (red line) and a fitted power profile (blue line).

The power law profile is described by:

$$U(z) = U_{30}\left(\frac{z}{30}\right)^{\alpha}$$

where U_{30} is the wind speed at 30m above the surface and α is the power-law constant. The fit given in Figure 3.1 has been obtained using least squares.

Figure 3.1 shows that the mean power law profile matches almost perfectly the mean observed vertical wind profile.
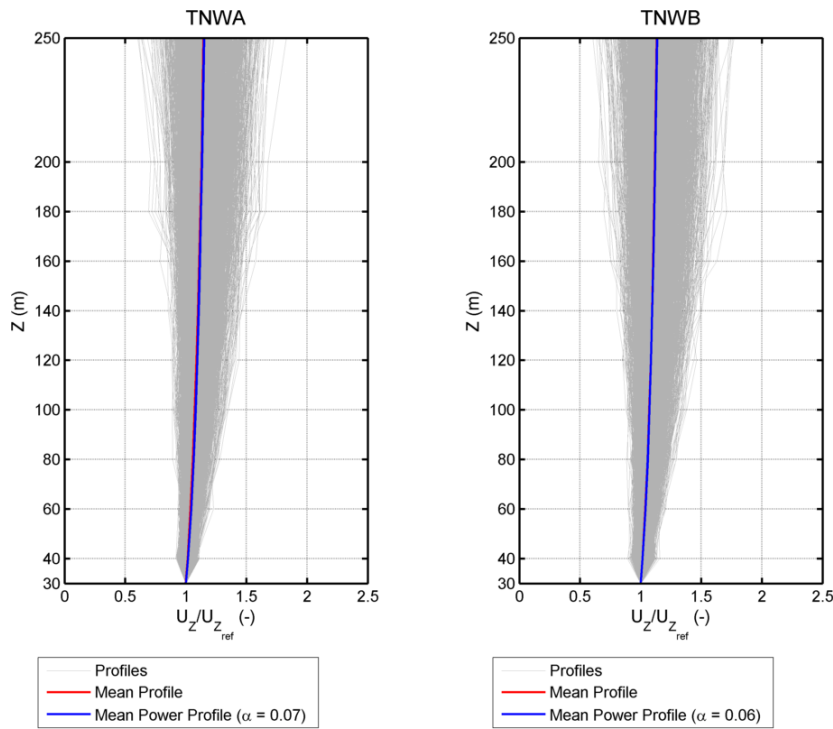
Figure 3.1: *Normalized LiDAR wind speed vertical profiles (data from December 2020).*

Figure 3.2 and Figure 3.3 show the timeseries of respectively the wind speed and direction at the observation levels. The figures show that the highest observed winds are from the South between the 25th and the 28th of December, peaking above 35 m/s at the higher levels and with large vertical wind speed gradients. The figures also show a long period of southern winds between the 13th and the 22th with also large vertical wind speed gradients.
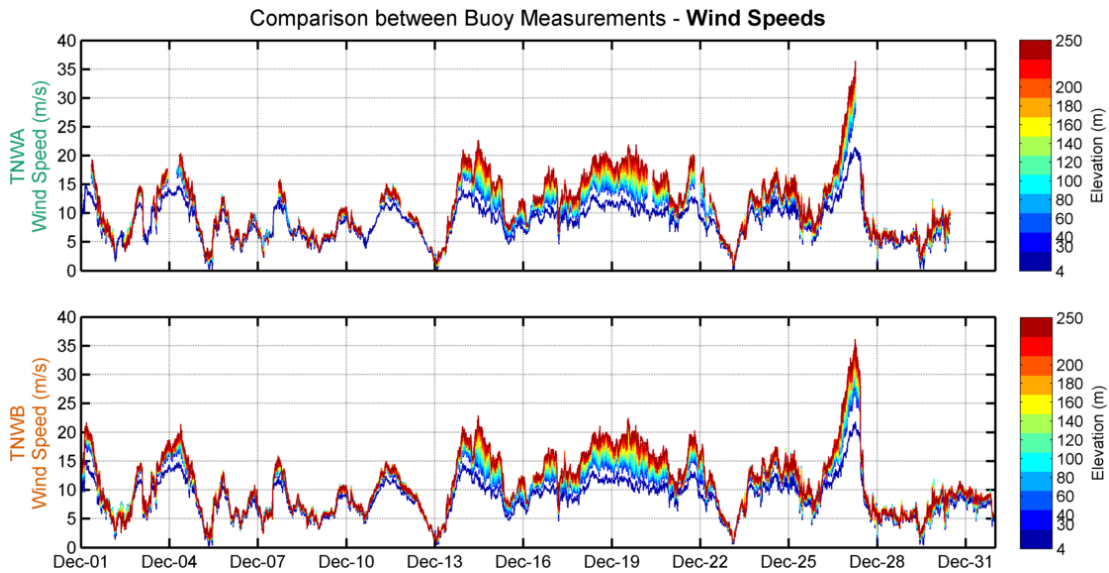
Figure 3.2: *Wind speeds (by elevation) at each buoy.*

Deltares
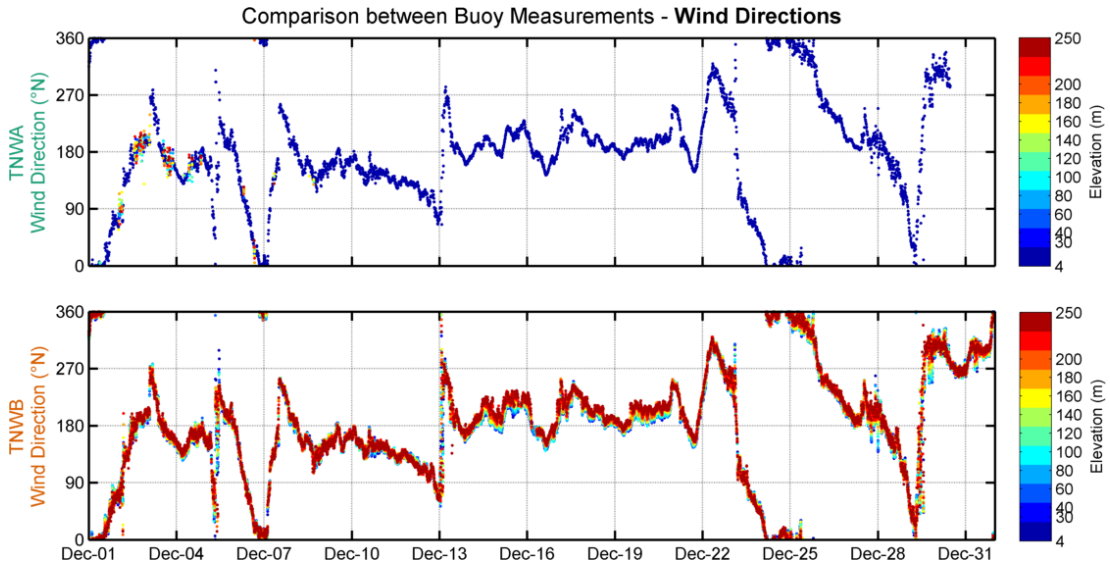
Figure 3.3: *Wind directions (by elevation) at each buoy.*

Figure 3.4 shows density scatter comparisons between the wind speed and direction measured by TNWA and TNWB at two chosen levels, 100m and 160m. The figure shows a general agreement between the observation of TNWA and TNWB, as could already be seen in figures 3.2 and 3.3.
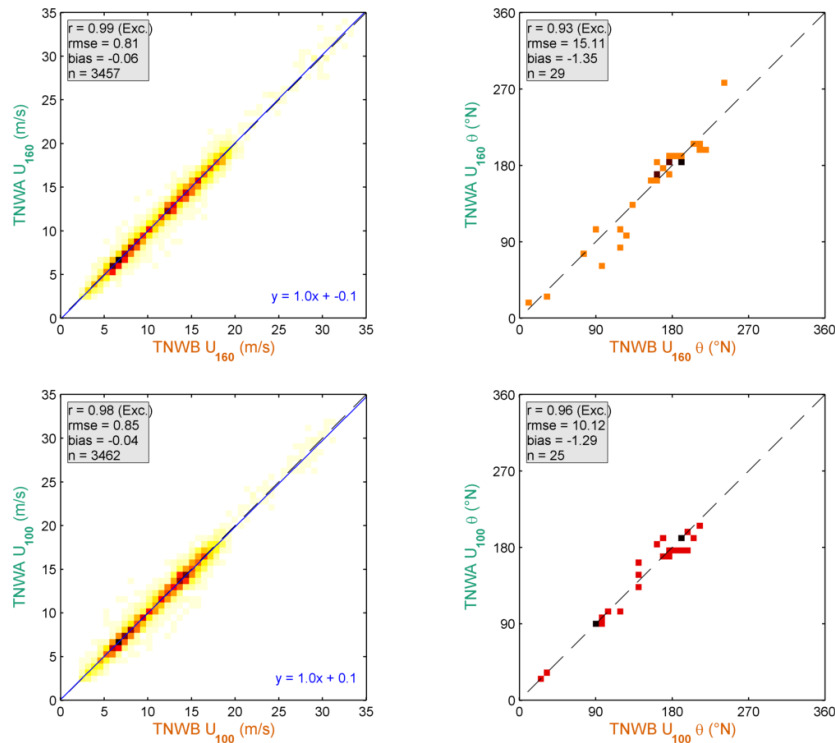
Figure 3.4: *Direct scatter comparison between LiDAR wind at 100 and 160 m (data from December 2020).*

In order to further quantify the differences between the TNWA and TNWB wind speed (and direction) observations, the slope, bias, correlations and square correlations between the TNWA and TNWB wind speed observations at all levels and the bias, correlations and square

correlations between the TNWA and TNWB wind direction observations at all levels have been computed considering all wind speeds above 2 m/s. These are given in Table 3.1 and (given the lower threshold) can be compared against the criteria given in IEC 61400-12-1 (2017) and IEA Wind (2017)[1]. The table shows that, even applying such a low wind speed threshold, the comparisons are at all levels excellent in terms of wind speed. Furthermore, the wind speed KPIs given in the table are in line those obtained during the pre-validation of the LiDARs, see e.g. DNV-GL (2019). (Recall that the wind direction data are given for completeness, but not commented given the too low sample sizes.)

Table 3.1: Statistical comparison between the winds from the LiDAR buoys with elevation.

	Wind Speed					Wind Direction			
Elev. (m)	r^2 (-)	r (-)	Bias (m/s)	Sym. Slope (-)	n (-)	r^2 (-)	r (-)	Bias (°)	n (-)
4	0.96	0.98	0.06	1.01	4139	0.96	0.98	-1.8	4139
30	0.96	0.98	-0.08	0.99	3638	0.84	0.92	-3.1	31
40	0.96	0.98	-0.07	0.99	3645	0.80	0.89	-0.2	21
60	0.96	0.98	-0.06	1.00	3637	0.89	0.94	-4.6	36
80	0.96	0.98	-0.05	1.00	3458	0.88	0.94	-0.8	29
100	0.97	0.98	-0.04	1.00	3462	0.92	0.96	-1.3	25
120	0.97	0.98	-0.05	1.00	3467	0.91	0.95	-3.9	27
140	0.97	0.99	-0.06	1.00	3463	0.69	0.83	0.7	27
160	0.97	0.99	-0.06	1.00	3457	0.87	0.93	-1.4	29
180	0.98	0.99	-0.07	1.00	3460	0.85	0.92	1.3	22
200	0.98	0.99	-0.08	1.00	3447	0.77	0.88	-3.9	23
250	0.98	0.99	-0.09	0.99	3449	0.87	0.94	-6.2	22

3.2 Validation

In this section the TNWA (Section 3.2.2) and TNWB (Section 3.2.3) wind data at a single level are validated against anemometer observations at L91 (at a height of z=87 m and at a distance of about d= 59 km from TNW), K13 (z=73.8 m, d=178 km), AWG (z=60 m, d=64 km), and HG (z=18 m, d=75 km). The wind speeds at several levels are validated against LiDAR observations at K13 (z=63, 91, 116, 141, 166, 191 and 241 m). Note that K13 is at a considerable distance from TNWA and TNWB and in periods with large spatial wind variations comparisons between these data can be expected to be poor. Furthermore, given its proximity to the coast, the winds blowing from the coast at HG and AWG are expected to be more strongly influenced by land effects. Nevertheless, data from these stations are still expected to show some correspondence with the TNW data and in any case to provide a measure of spatial variability and also variability in height.

An overview of the comparisons between the TNW and the fixed platform anemometer datasets is presented first, followed by a comparison of each TNWA and TNWB datasets with measured fixed platform anemometer and LiDAR data. Finally, the spatial variability of the wind is evaluated using model data.

3.2.1 Overview

Figure 3.5 provides an overview of the comparisons, comparing the timeseries of the L91, K13, AWG, and HG observations and the TNWA and TNWB LiDAR observations at the levels closer to those of the anemometers. A further overview of the comparisons between data at the buoy and platform locations is given by means of wind roses at Figure 3.6. Given the

---

[1]Note that the applied T-linear correlation coefficient Equation 1.3 leads in general to slightly lower correlations between directions than those using the standard correlation as in the cited criteria.

Deltares

lack of wind direction data, Figure 3.6 contains no TNWA nor K13 roses. The roses show a general alignment between the datasets and that the most predominant and stronger winds during this period are from the South, with a more southwestern alignment at AWG.
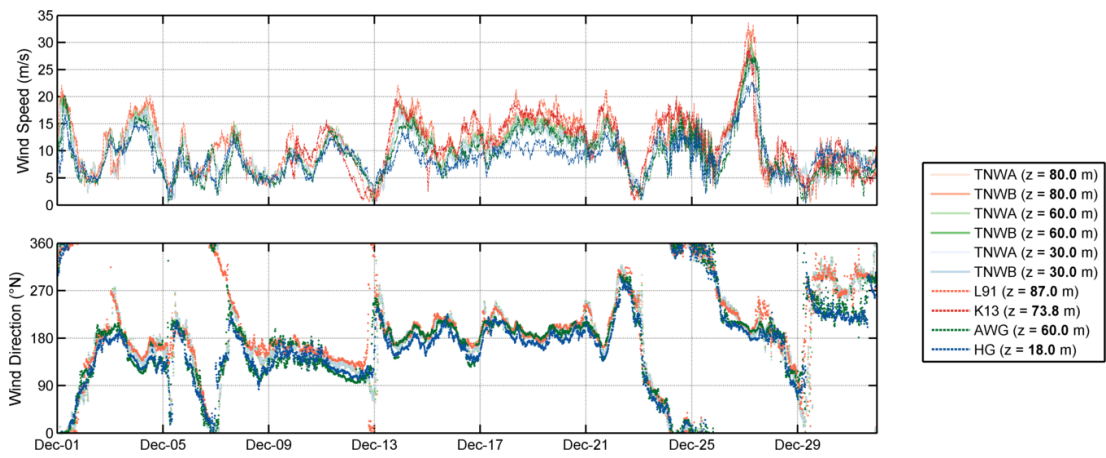
Figure 3.5: Wind speed and direction for all locations (data from December 2020).
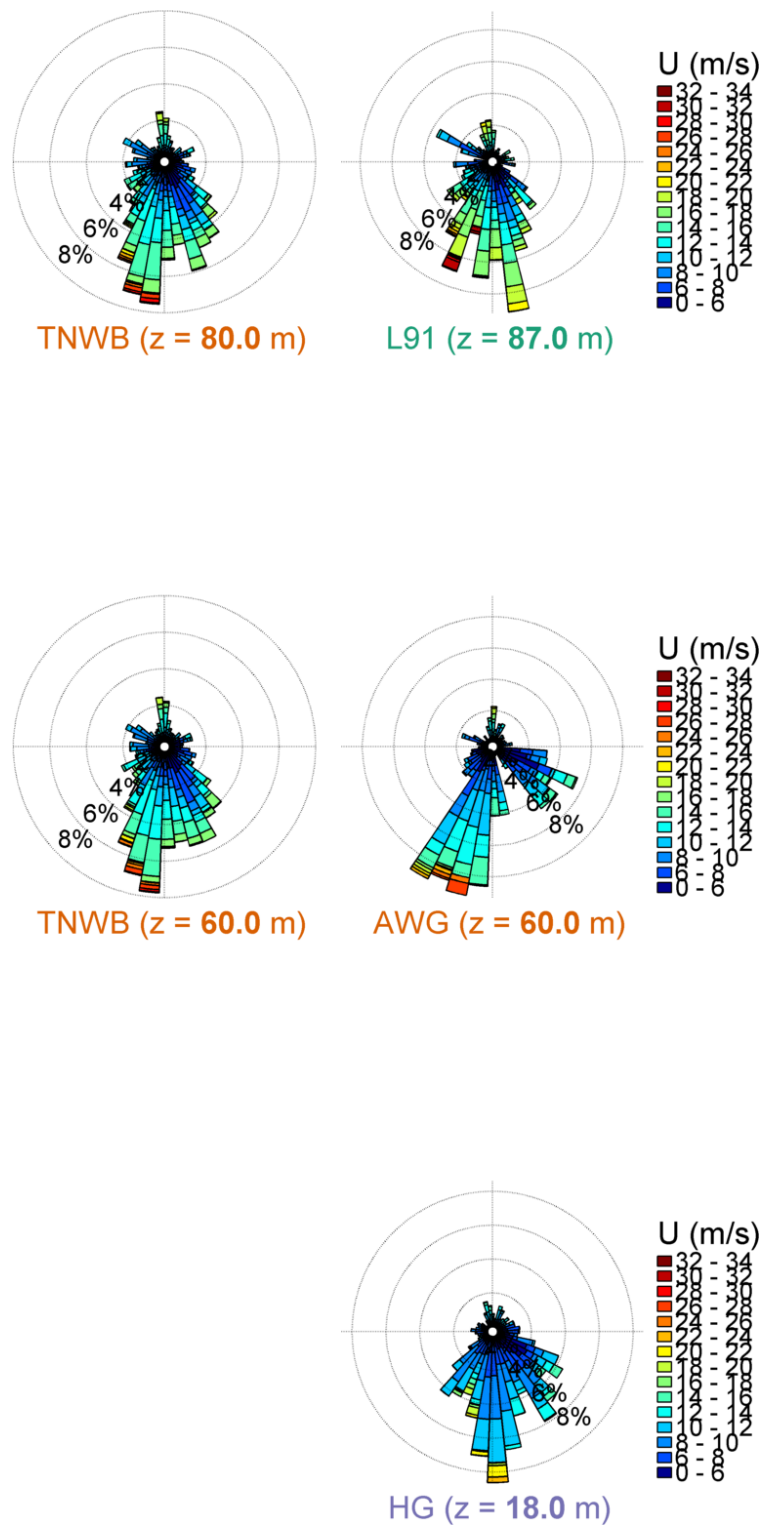
Figure 3.6: *Wind roses (of bin width 8°) for all locations with good availability of wind direction data (December 2020).*

3.2.2 Ten Noorden van de Waddeneilanden Buoy TNWA

3.2.2.1 Anemometer

Figures 3.7, 3.8, 3.9 and 3.10 show comparisons between TNWA observations and those at L91, K13, AWG, and HG, respectively. The correlation, root-mean-square error and bias statistics are printed in the figures. As can be seen in the figures, the comparisons between the TNWA wind speed observations and those from L91 are excellent, those from K13 and AWG are good and those from HG are reasonable. The lower correlations with the observations from HG appear to be due to local HG effects when the winds blow from the South. (Given the low availability of TNWA wind direction data, the wind direction comparisons are not analysed.)
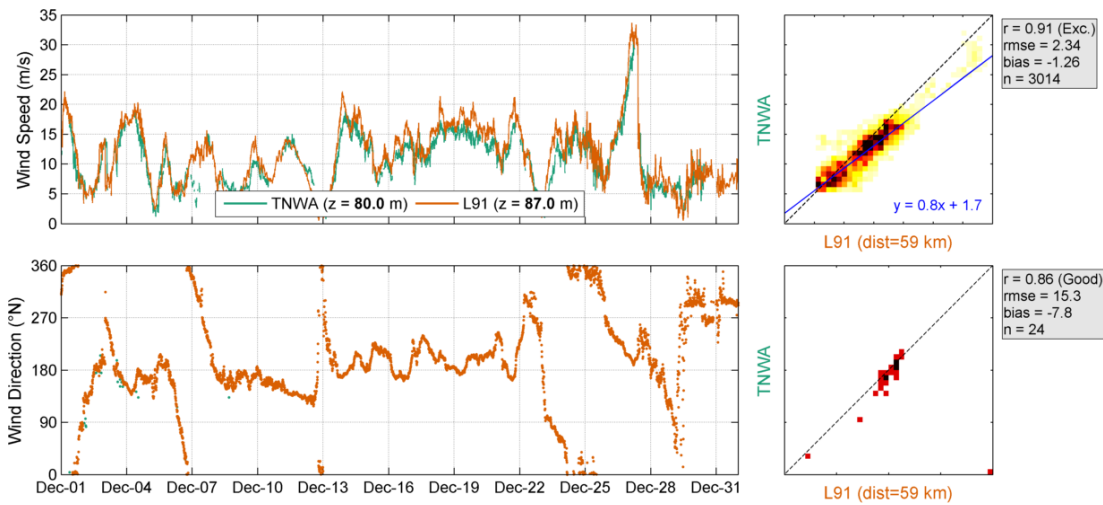
Figure 3.7: *Validation of TNWA (data from December 2020) with L91 wind data. Left panel: Timeseries. Middle panel: Density scatter, with the darker colours indicating more data density.*
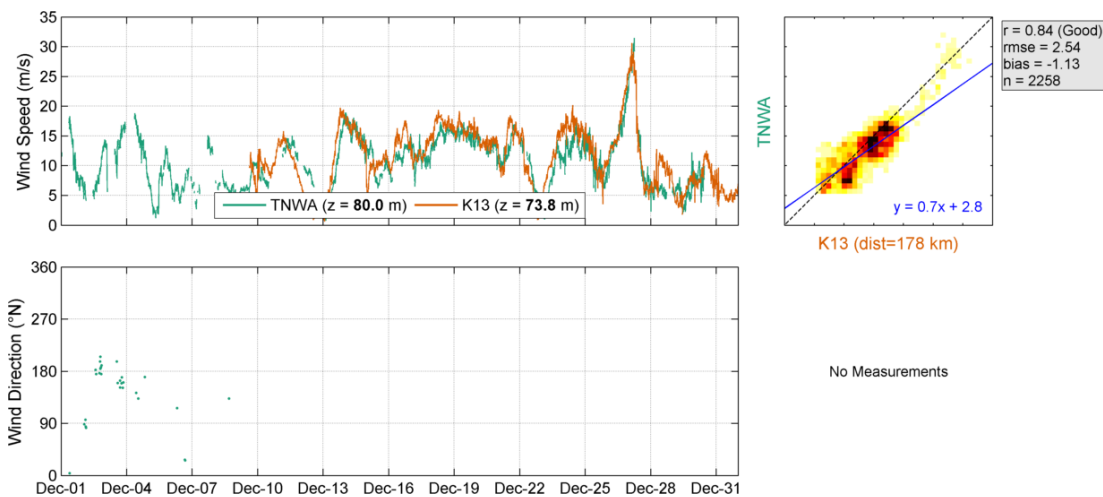
Figure 3.8: *Validation of TNWA (data from December 2020) with K13 wind data. Left panel: Timeseries. Middle panel: Density scatter, with the darker colours indicating more data density.*
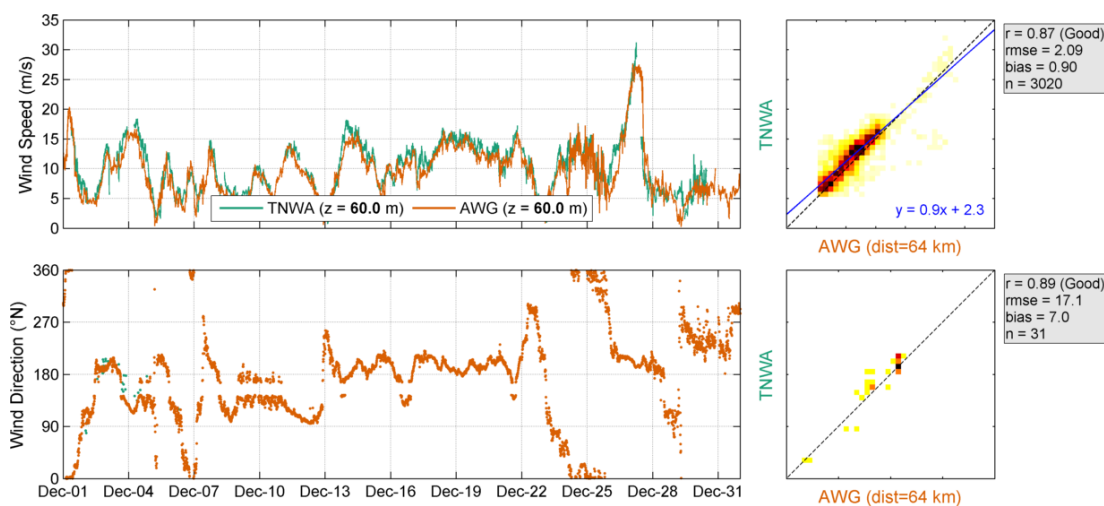
Figure 3.9: *Validation of TNWA (data from December 2020) with AWG wind data. Left panel: Timeseries. Middle panel: Density scatter, with the darker colours indicating more data density.*
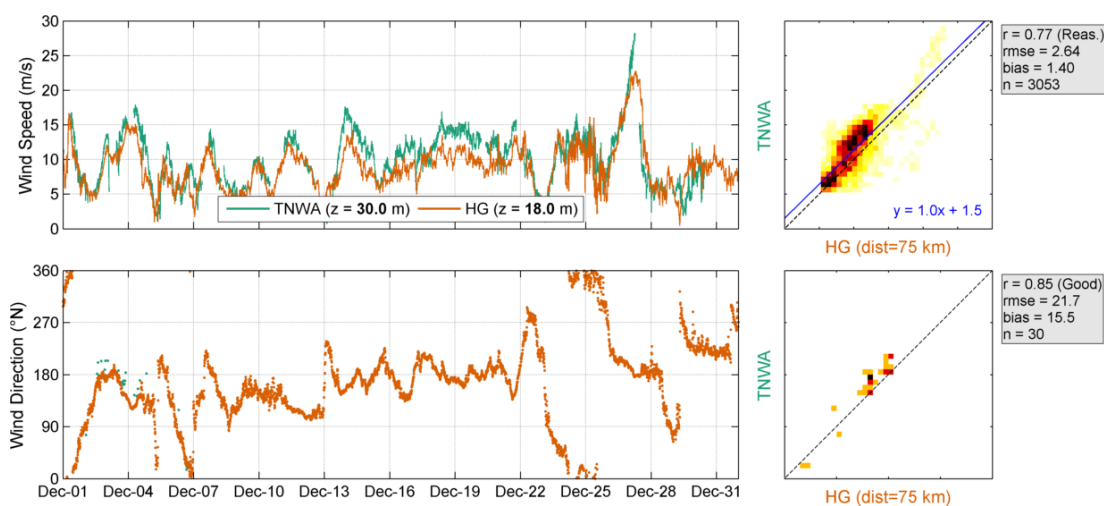
Figure 3.10: *Validation of TNWA (data from December 2020) with HG wind data. Left panel: Timeseries. Middle panel: Density scatter, with the darker colours indicating more data density.*

3.2.2.2 LiDAR

In the following the TNWA wind data are compared with the LiDAR observations at K13. Before comparing the TNWA data with the K13 LiDAR data, these are validated against the anemometer data at K13. Figure 3.11 shows the comparison between the K13 LiDAR and anemometer timeseries. A timeseries comparison is provided (by elevation), with a density scatter comparing the best match (in terms of elevation) between the two datasets. I.e., the LiDAR measurements at the 63 m level are directly compared against the anemometer observations at the 73.8 m level. Note that the K13 anemometer wind speed observations are only available from the 10th and there are no wind directions available. The wind speed correlations are excellent, but as expected due to the difference in elevation (73.8 and 63 m), there is a bias, with the (observed at a higher height) anemometer wind speeds being on average higher.

Table 3.2 shows the comparisons between the TNWA observations and those of the closer

vertical levels by the LiDAR at K13. As was also the case in the comparisons with the K13 anemometer, the wind speed comparisons are good at all levels.
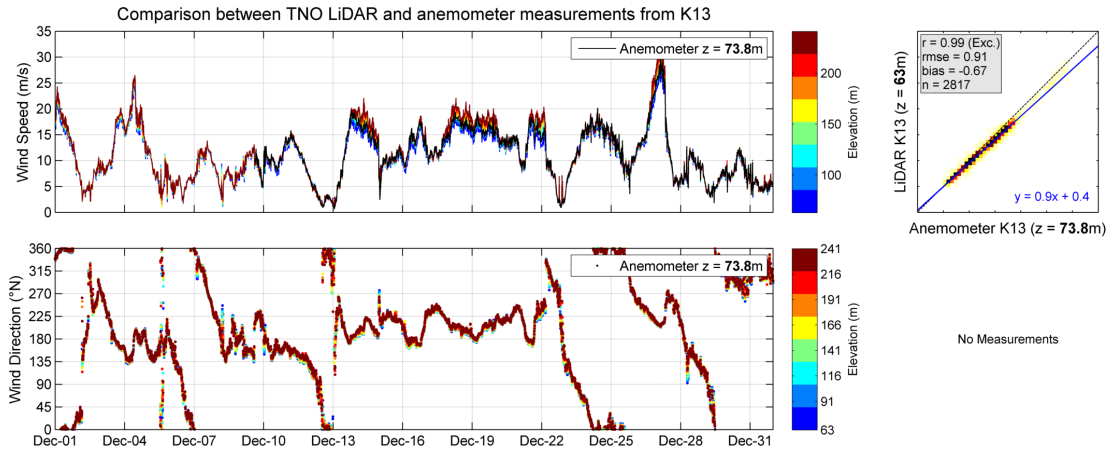
Figure 3.11: *Comparison between LiDAR and anemometer measurements at K13.*

Table 3.2: *Statistical comparison between TNWA and K13 LiDARs at different heights.*

Elevation		Wind Speed				Wind Direction		
TNWA (m)	K13 (m)	r (-)	Bias (m/s)	Symmetrical Slope (-)	n (-)	r (-)	Bias ($^\circ$)	n (-)
60	63	0.81	0.73	1.07	3078	0.46	27.0	32
100	91	0.82	0.66	1.05	2946	0.24	20.4	20
120	116	0.82	0.67	1.05	2954	0.35	19.0	23
140	141	0.83	0.67	1.05	2962	0.23	42.0	23
160	166	0.83	0.64	1.05	2953	0.57	27.7	24
200	191	0.84	0.48	1.03	2946	0.46	23.5	20
250	241	0.85	0.48	1.03	2934	0.84	25.4	18

3.2.3   Ten Noorden van de Waddeneilanden Buoy TNWB

3.2.3.1   Anemometer

As shown for TNWA, figures 3.12, 3.13, 3.14 and 3.15 show comparisons between TNWB observations and those at L91, K13, AWG, and HG, respectively. The correlation, root-mean-square error and bias statistics are printed in the figures. As was the case in the comparisons between the TNWA and the fixed stations wind speeds, the comparisons between the TNWB wind speed observations and those from L91 are excellent, those from K13 and AWG are good and those from HG are reasonable. The comparisons between the TNWN and the fixed stations wind directions are good for all stations with data available (only missing from K13).
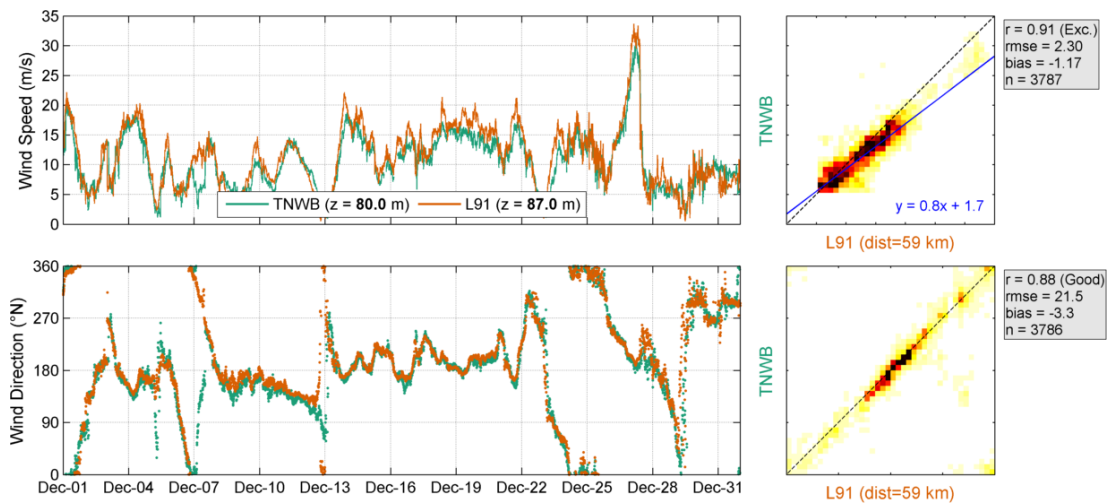
Figure 3.12: *Validation of TNWB (data from December 2020) with L91 wind data. Left panel: Timeseries. Middle panel: Density scatter, with the darker colours indicating more data density.*
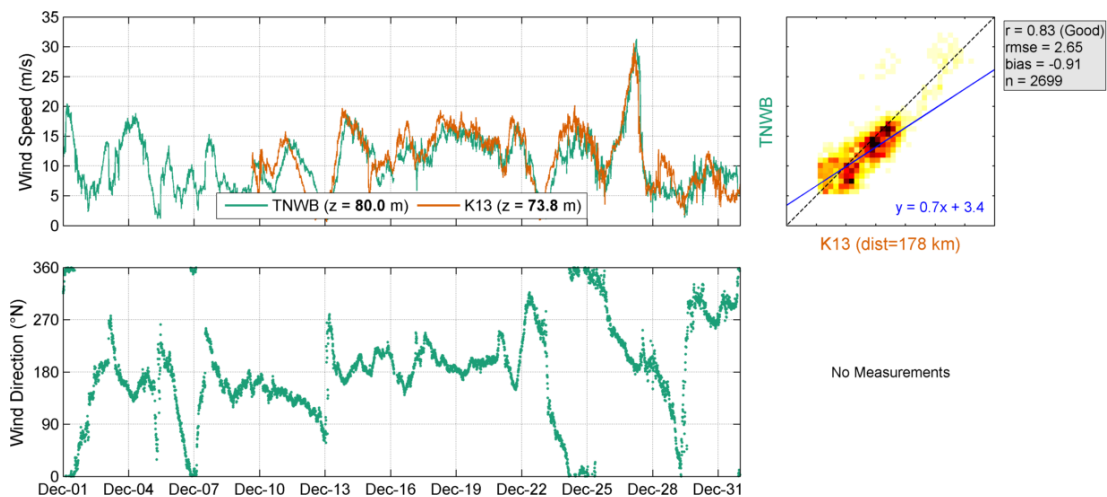

Figure 3.13: *Validation of TNWB (data from December 2020) with K13 wind data. Left panel: Timeseries. Middle panel: Density scatter, with the darker colours indicating more data density.*
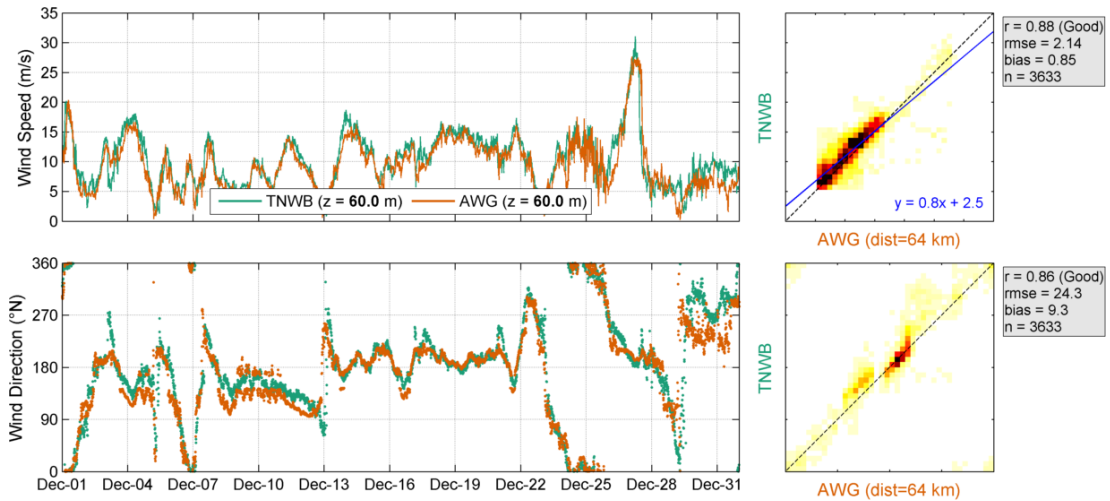
Figure 3.14: *Validation of TNWB (data from December 2020) with AWG wind data. Left panel: Timeseries. Middle panel: Density scatter, with the darker colours indicating more data density.*
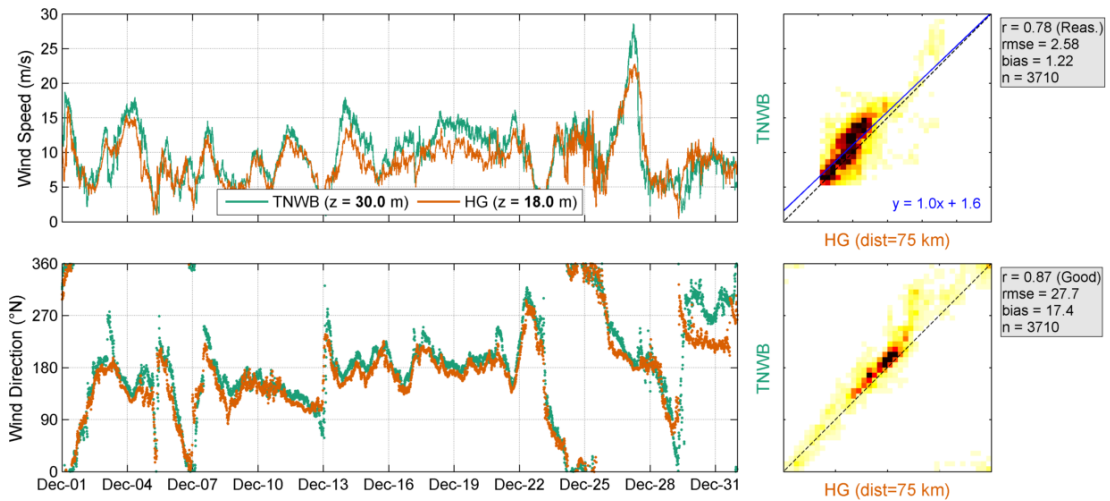
Figure 3.15: *Validation of TNWB (data from December 2020) with HG wind data. Left panel: Timeseries. Middle panel: Density scatter, with the darker colours indicating more data density.*

3.2.3.2 LiDAR

Table 3.3 show the error statistics between the TNWB observations and those of the closer vertical levels by the LiDARs at K13. As was also the case in the comparisons between the K13 and the TNWA data, the comparisons are at all levels good in terms of wind speed. In terms of wind direction the comparisons are reasonable to good.

***Table 3.3:** Statistical comparison between TNWB and K13 LiDARs at different heights.*

Elevation		Wind Speed				Wind Direction		
TNWB (m)	K13 (m)	r (-)	Bias (m/s)	Symmetrical Slope (-)	n (-)	r (-)	Bias (°)	n (-)
60	63	0.80	0.64	1.05	3657	0.75	9.7	3657
100	91	0.81	0.52	1.04	3635	0.77	9.1	3634
120	116	0.81	0.54	1.04	3646	0.78	8.2	3646
140	141	0.82	0.53	1.04	3658	0.78	7.9	3658
160	166	0.82	0.52	1.04	3656	0.79	8.3	3655
200	191	0.83	0.40	1.02	3641	0.79	8.0	3640
250	241	0.84	0.37	1.02	3630	0.80	8.5	3630

3.2.4 Spatial and temporal variability

In order to further evaluate the spatial variations in the observation period, the wind fields from the Dutch Meteorological Institute (KNMI) operational Numerical Weather Prediction model Hirlam7.2 are also considered. The model fields are only available at 10 m and with an hourly resolution. The spatial resolution of the model is about 11 km x 11 km, which implies that the model in principle underestimates the spatial variations and coastal effects, i.e. the model results can be expected to be smoother than the true fields.

In order to characterize further the most extreme event in the observation period, Figure 3.16 and Figure 3.17 show the model wind fields at the hour of the maximum observed 100 m wind speed at TNWA and at TNWB, respectively, which was observed at 5:00 on the 27th of December at TNWA and 70 minutes later at TNWB. The figures shows a peak wind event from the South/Southwest with the higher model wind speeds along the TNW, K13 and L91 locations.
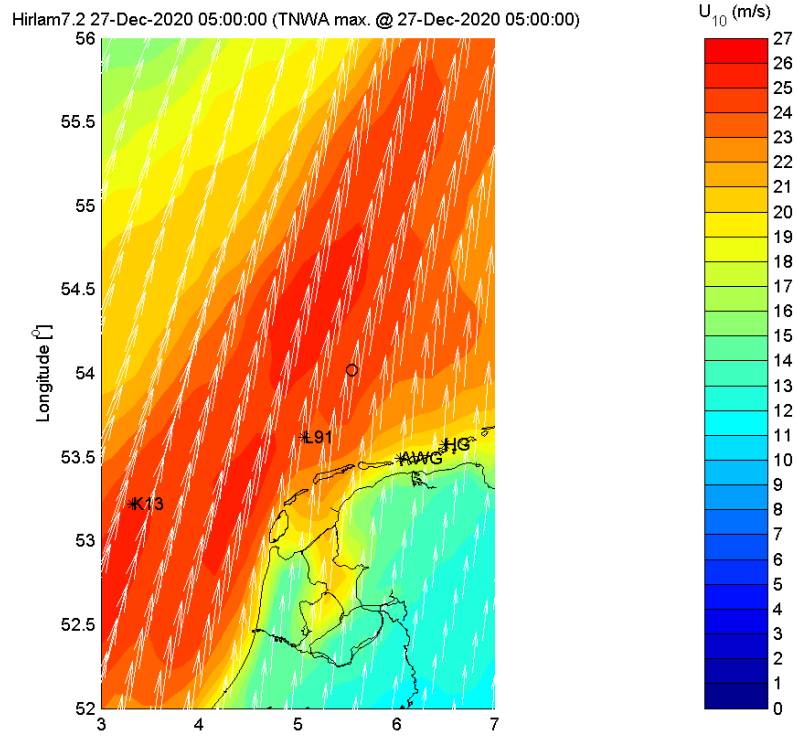
Figure 3.16: *Hirlam7.2 surface (10 m) wind field at the hour of the maximum TNWA 100 m wind speed. The *s indicate the locations of the fixed stations and the ○s the TNW locations.*
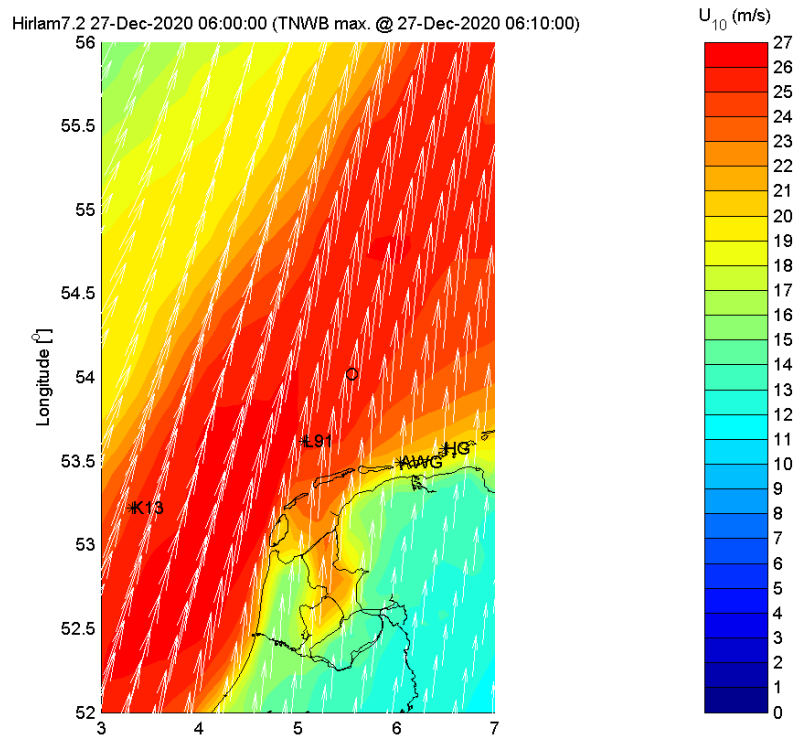
**Figure 3.17:** *Hirlam7.2 surface (10 m) wind field at the hour of the maximum TNWB 100 m wind speed. The *s indicate the locations of the fixed stations and the ○s the TNW locations.*

Table 3.4 shows the correlations between the Hirlam7.2 10 m (hourly) wind speeds and directions from the model grid points closer to the buoy and the fixed station locations at the timestamps at which the data from each of the buoys are valid. Given the proximity of the TNWA and TNWB locations the considered model grid point is the same, therefore differences between correlations with the data at the TNWA and TNWB locations are only due to differences in measurement data availability. For these periods the corresponding correlations between the buoy and the fixed station anemometer (10 minute) observations (at the closer vertical levels) are given in figures 3.7 to 3.10 and 3.12 to 3.15 and reproduced Table 3.5. As can be seen in Table 3.4, the model winds at TNW have the higher correlations with the winds at the L91 and AWG locations and the lowest with the winds at K13. The correlations between the model winds at TNW and HG are higher than between the observations because the model winds are not as influenced by the local effects observed at HG. In summary, the comparison of the correlations between the observations and the models results confirm that the found discrepancies are mostly due to spatial variations (note also the lower correlations between the TNW and K13) and local effects (as noted at HG), which are less present in the model results.

Table 3.4: Statistical comparison between the model results at the buoy and at the fixed station locations at the timestamps at which the buoy data are valid

	TNWA			TNWB		
Station	U_{10} r **(-)**	U_{dir} r **(-)**	n **(-)**	U_{10} r **(-)**	U_{dir} r **(-)**	n **(-)**
L91	0.97	0.94	533	0.96	0.91	664
K13	0.81	0.80	533	0.79	0.80	664
AWG	0.89	0.92	533	0.89	0.92	664
HG	0.84	0.88	533	0.85	0.87	664

Table 3.5: Statistical comparison between the TNWA and TNWB buoy observations and those from the fixed stations.

	TNWA				TNWB			
Station	U_{h} r **(-)**	n **(-)**	U_{dir} r **(-)**	n **(-)**	U_{h} r **(-)**	n **(-)**	U_{dir} r **(-)**	n **(-)**
L91	0.91	3014	0.86	24	0.91	3787	0.88	3786
K13	0.84	2258	-	0	0.83	2699	-	0
AWG	0.87	3020	0.89	31	0.88	3633	0.86	3633
HG	0.77	3053	0.85	30	0.78	3710	0.87	3710

3.3 Conclusions

Based on the comparisons between the wind speed data from the buoys, which are excellent at all levels and within the best practice range (and in accordance with KPIs obtained during the pre-validation of the LiDARs), the validation of the TNWA wind speeds and TNWB wind speeds and directions against observations and model data, which shows mismatches can be explained by local effects and spatial and vertical variations, it can be concluded that the accuracy of the TNWA and TNWB wind speeds and TNWB wind directions is high.

4 Waves

The measured waves from both buoys are presented and analyzed within this chapter. The goal is to assess the reliability and accuracy of the retrieved wave data from both TNWA and TNWB. This is completed by first comparing the integral parameters from both buoys against each other, followed by a statistical validation against fixed wave measurements in the area.

4.1 Ten Noorden van de Waddeneilanden description and intercomparison

The timeseries of the main wave parameters for both TNWA and TNWB is shown in Figure 4.1. It includes the following parameters:

- significant wave height, H_s
- peak wave period, T_p
- mean wave direction, MWD
- swell and sea[1] significant wave heights, H_{sswell} and H_{ssea}
- maximum wave height, H_{max}
- swell and sea mean wave directions, MWD_{swell} and MWD_{sea}
- mean wave periods, T_{m01} and T_{m02}, and
- swell and sea mean wave periods, $T_{m02swell}$ and T_{m02sea}.

Figure 4.1 shows that the TNWA and TNWB signals are near-identical (e.g. H_s, T_{m02}, etc . . .) with only short term discrepancies between T_p and the mean wave direction of swell. These are expected given the generally low conditions and that these parameters depend more strongly on the sampling variability (randomness of the sea surface elevation) and discreteness of the wave spectra. Figure 4.1 also shows that during this period the highest observed waves are from the Southwest on the 27th, in line with the period of highest winds.

---

[1]The swell and sea variables are computed from the spectral energy in the frequency band between respectively 0.04 and 0.10 Hz and 0.10 and 0.50 Hz (cf. Table 2.1).
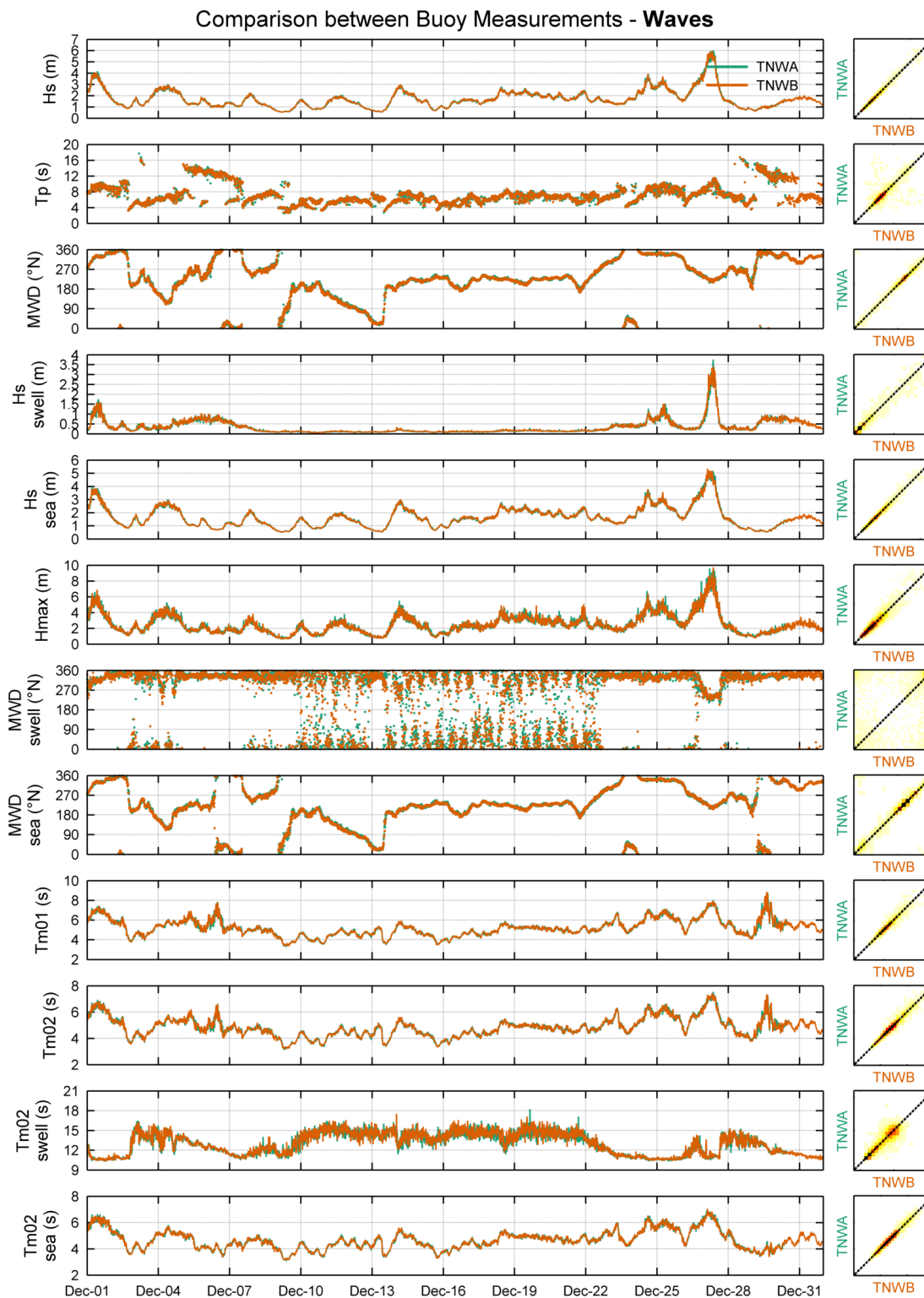
Figure 4.1: *Wave parameters at each buoy (data from December 2020).*

The slope, bias, correlations and square correlations were calculated for all wave parameters measured at TNWA and TNWB to quantify their statistical differences, see Table 4.1. As can be seen in the table, the agreement between the two buoys is excellent in terms of all parameters, except in terms of peak wave period which is reasonable and swell mean wave direction which is poor. The mismatches in the mean wave direction of swell are in periods

with almost no swell energy (cf. Figure 4.1). These low levels of energy explain the variability in the resulting swell direction but also make it less important.

Table 4.1: Statistical comparison between TNWA and TNWB wave parameters.

Parameter	Unit	r^2 (-)	r (-)	Bias (unit)	Symmetrical Slope (-)	n (-)
hm0	m	0.98	0.99	0.00	1.00	4245
tp	s	0.60	0.78	-0.00	1.00	4245
mdir	°N	0.96	0.98	-0.57	1.00	4245
hm0a	m	0.94	0.97	0.01	1.03	4244
hm0b	m	0.98	0.99	0.00	1.00	4245
hmax	m	0.89	0.94	-0.00	0.99	4245
mdira	°N	0.14	0.38	-2.77	1.00	4245
mdirb	°N	0.94	0.97	-0.81	1.00	4245
tm01	s	0.94	0.97	0.00	1.00	4245
tm02	s	0.95	0.97	-0.00	1.00	4245
tm02a	s	0.81	0.90	0.07	1.01	4245
tm02b	s	0.96	0.98	-0.01	1.00	4245

4.2 Validation

An overview of the comparisons is first presented, followed by a detailed comparison between the data from TNWA (Section 4.2.2) and TNWB (Section 4.2.3) with the fixed observations.

4.2.1 Overview

Figure 4.2 and Figure 4.3 show the significant wave height and peak wave period roses, respectively, at TNWA, TNWB and SON. No roses are shown for F3 because there are no wave direction observations available from F3. The roses show an overall agreement, especially when considering their locations. At TNW the severer and most predominant waves are from the Southwest. Waves from the North have longer periods and also a high frequency of occurrence. Given its location nearer the shore (cf. Figure 1.2) and local refraction, waves from Southwest at TNW have a more northern alignment at SON.

Comparison between Buoy Measurements - **Waves**
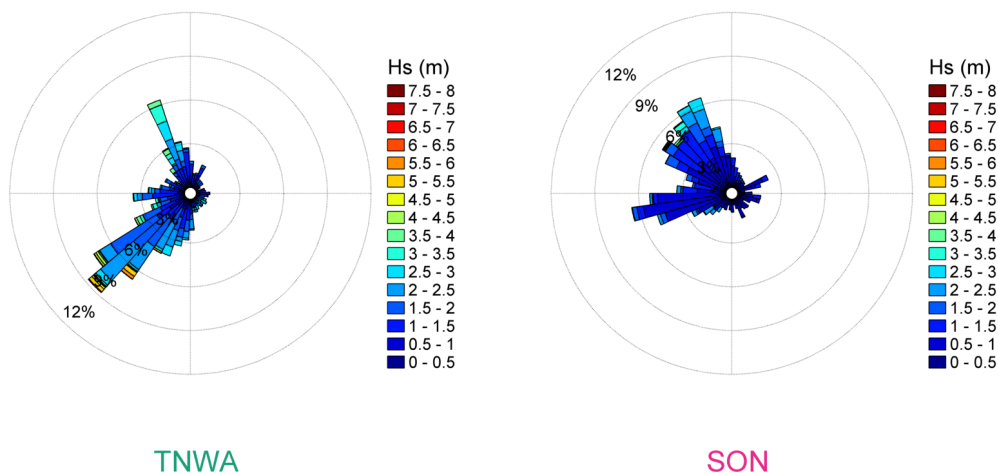
Figure 4.2: Significant wave height roses (data from December 2020).

Comparison between Buoy Measurements - **Waves**
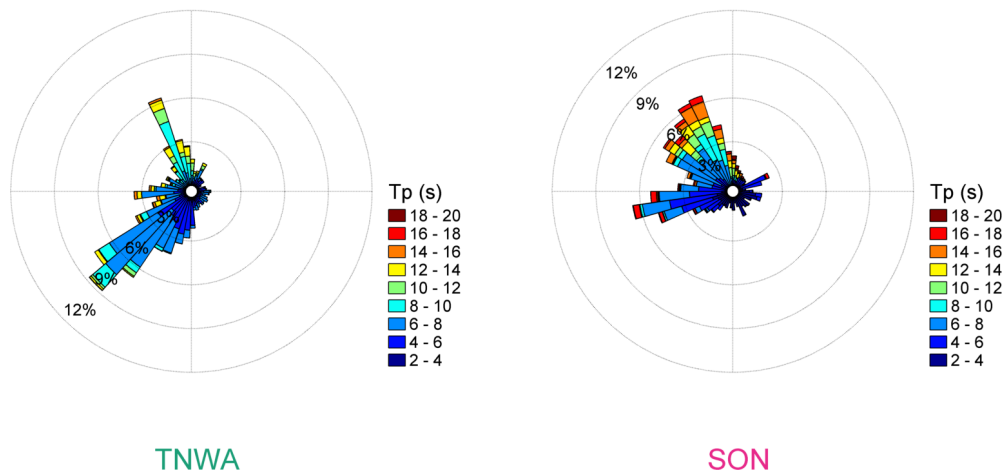
Figure 4.3: *Peak wave period roses (data from December 2020).*

4.2.2 Ten Noorden van de Waddeneilanden Buoy TNWA

Figures 4.4 and 4.5 show comparisons between TNWA observations and those at F3 and SON of H_s, T_p, mean wave period, $T_{m0,2}$, and mean wave direction, MWD (only SON, Figure 4.5). The correlation, root-mean-square error and bias statistics are printed in each of the figures.

As can be seen in the figures, the comparisons between TNWA observations and those:

- from F3 are excellent in terms of significant and swell wave height, good in terms of mean wave period and reasonable in terms of peak wave period; and
- from SON are reasonable in terms of significant and swell wave height and poor in terms of peak and mean wave period and mean wave direction, with the high southwestern waves reaching TNW and F3 not reaching the SON location.

Discrepancies between the waves at TNW and SON are expected given the shallower and closer to the shore location of SON (cf. Figure 1.2). Discrepancies in terms of peak wave period between the data from all locations are also expected given the discrete characteristics of the variable.
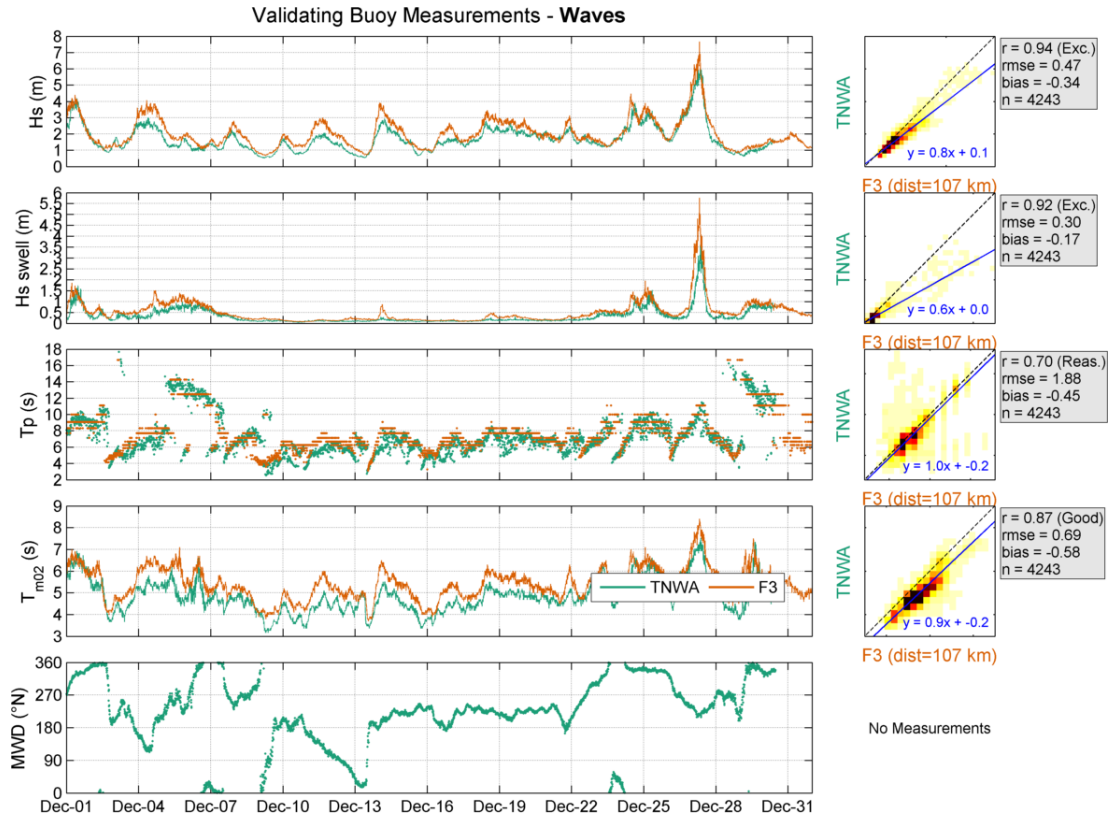
Figure 4.4: *Validation of TNWA (data from December 2020) with F3 wave data. Left panel: Timeseries. Middle panel: Density scatter, with the darker colours indicating more data density.*
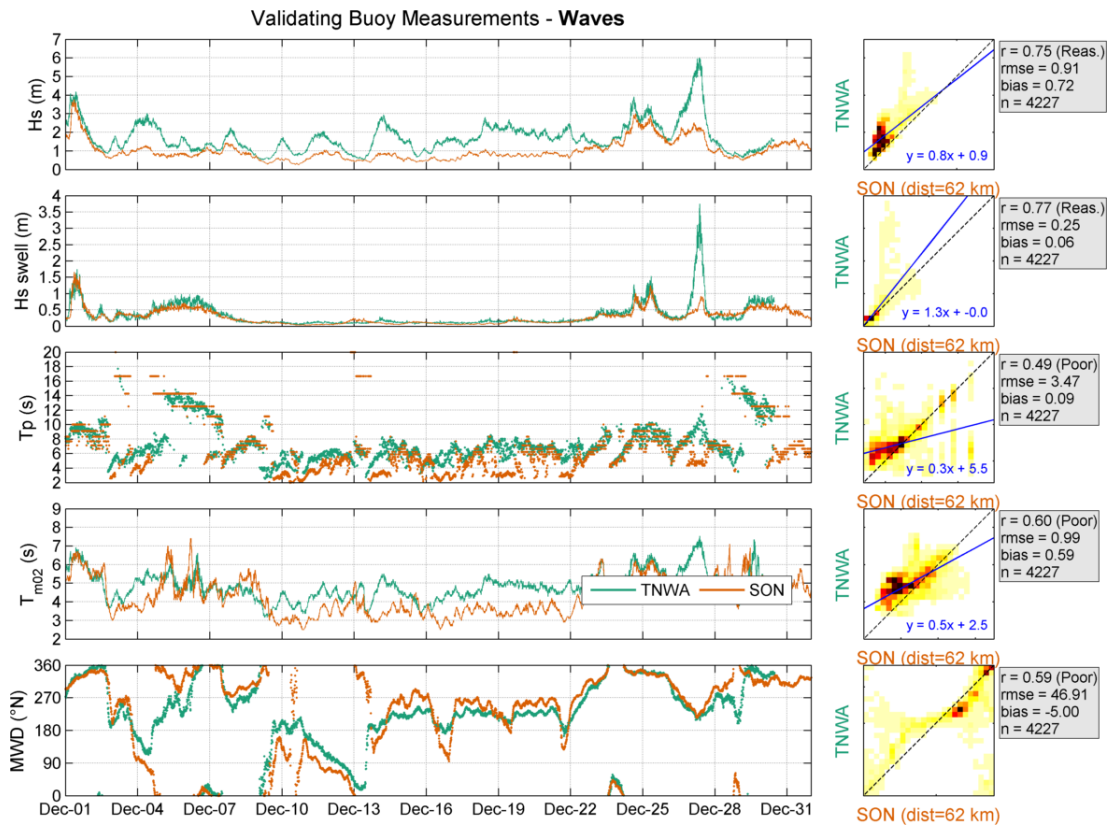
Figure 4.5: *Validation of TNWA (data from December 2020) with SON wave data. Left panel: Timeseries. Middle panel: Density scatter, with the darker colours indicating more data density.*

4.2.3 Ten Noorden van de Waddeneilanden Buoy TNWB

Figures 4.6 and 4.7 show comparisons between TNWB observations and those at F3 and SON of H_s, T_p, mean wave period, $T_{m0,2}$, and mean wave direction, MWD (only SON, Figure 4.7). The correlation, root-mean-square error and bias statistics are printed in each of the figures. The comparisons between the TNWB and the fixed station data are in line with those between the TNWA and the fixed station data.
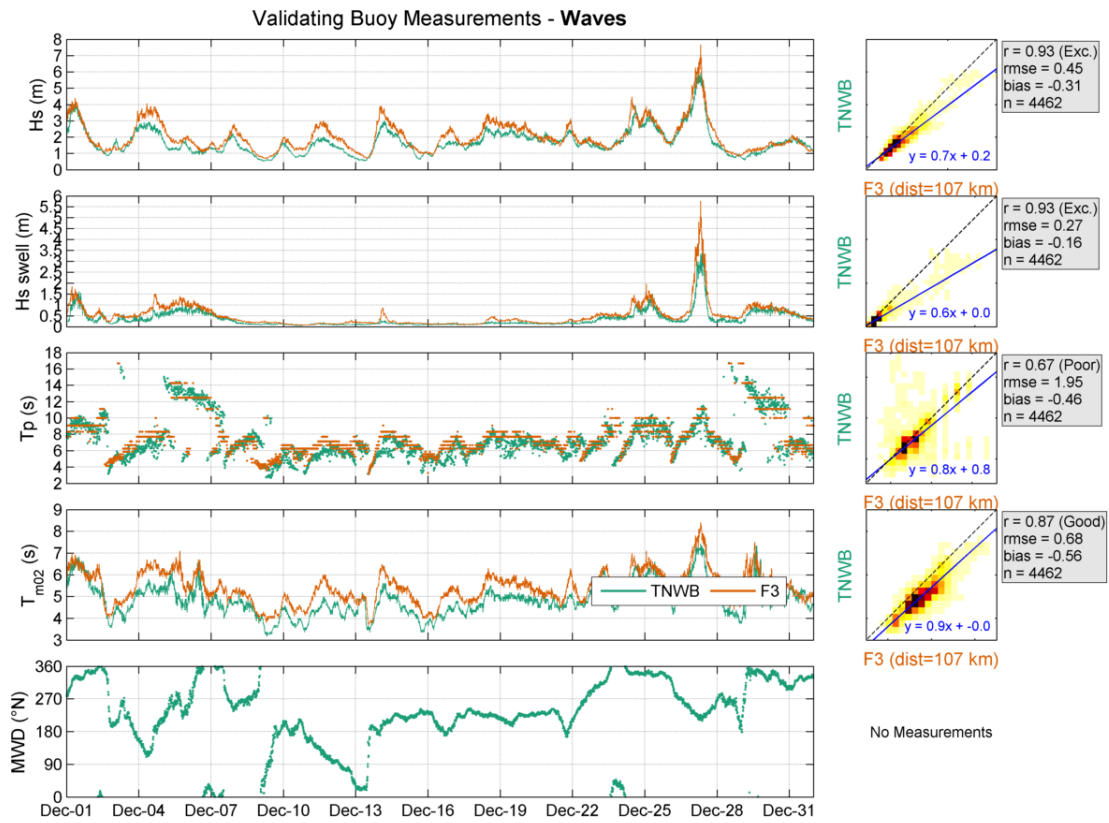
Figure 4.6: *Validation of TNWB (data from December 2020) with F3 wave data. Left panel: Timeseries. Middle panel: Density scatter, with the darker colours indicating more data density.*
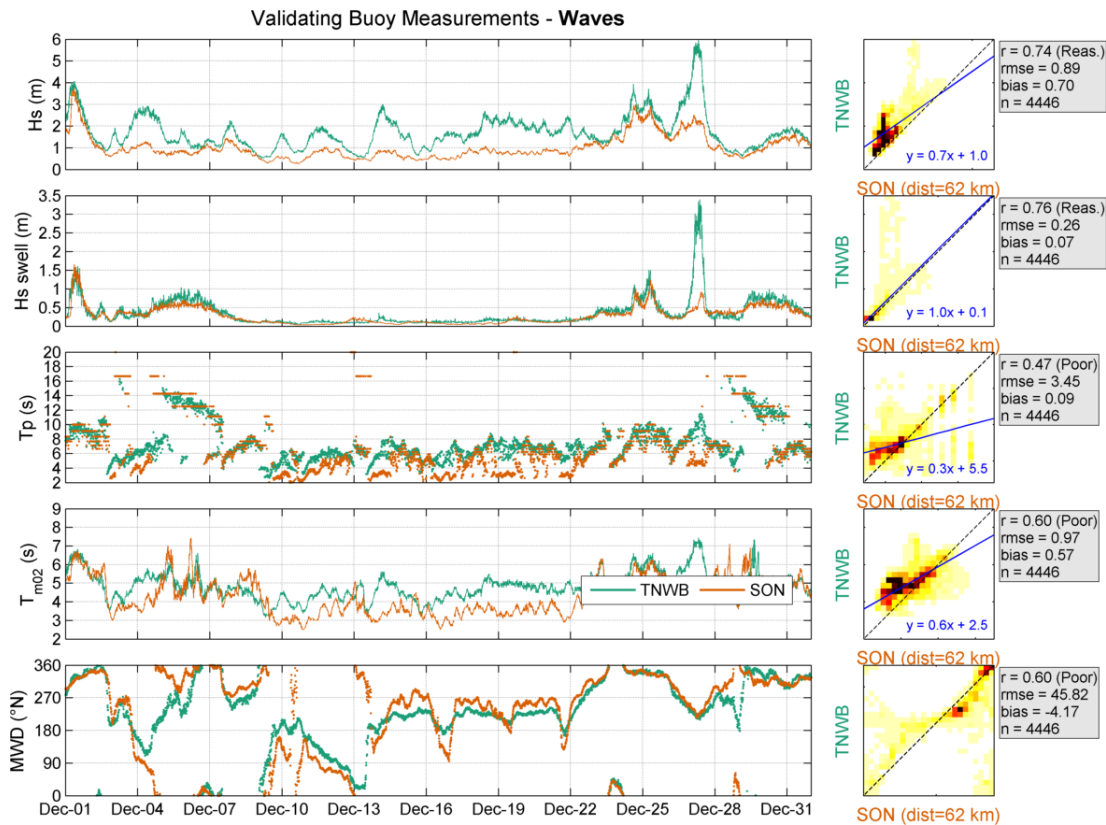
Figure 4.7: *Validation of TNWB (data from December 2020) with SON wave data. Left panel: Timeseries. Middle panel: Density scatter, with the darker colours indicating more data density.*

4.3 Summary and conclusions

The correlations between the buoy and the fixed station wave observations given in figures 4.4 to 4.5 and 4.6 to 4.7 are summarized in Table 4.2.

Table 4.2: *Statistical comparison between the TNWA and TNWB buoy observations and those from the fixed stations.*

	TNWA		TNWB	
Station	**F3**	**SON**	**F3**	**SON**
H_s r **(-)**	0.94	0.75	0.93	0.74
H_s n **(-)**	4243	4227	4462	4446
H_{sswell} r **(-)**	0.92	0.77	0.93	0.76
H_{sswell} n **(-)**	4243	4227	4462	4446
T_p r **(-)**	0.70	0.49	0.67	0.47
T_p n **(-)**	4243	4227	4462	4446
T_{m02} r **(-)**	0.87	0.60	0.87	0.60
T_{m02} n **(-)**	4243	4227	4462	4446

Based on a) the comparisons between the data from the buoys, which are excellent for all parameters, except as expected those depending strongly on the sampling variability (randomness of the sea surface elevation) and discreteness of the wave spectra (T_p and MWD_{swell}, cf. Table 4.1), and b) the validation of the data against the fixed station observations, in which mismatches can be explained by local effects, spatial variations and again discreteness of the wave spectra, it can be concluded that the accuracy of the TNW

buoy wave data is high.

5 Temperature

During this deployment period air and surface water temperatures are measured at both buoys (cf. Figure 2.1).

5.1 Ten Noorden van de Waddeneilanden intercomparison

Figure 5.1 shows the observed air and water temperature and their differences. All signals align.
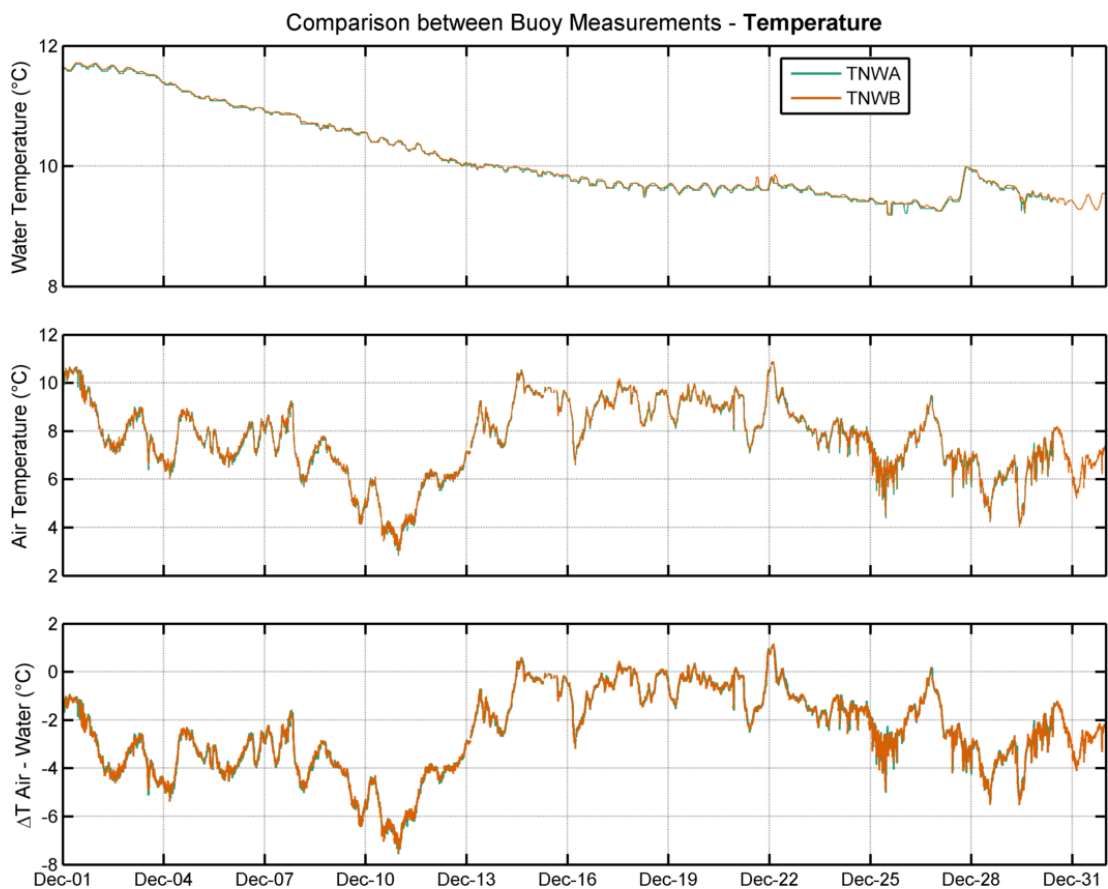

Figure 5.1: *Temperature difference measured at LiDAR buoys (data from December 2020).*

5.2 Validation

The comparisons between fixed station measurements and the TNW data are presented in Section 5.2.1 (water temperature) and in Section 5.2.2 (air temperature).

5.2.1 Water Temperature

A timeseries comparison between the observations from both buoys and sensors and the fixed stations is presented in Figure 5.2. The water temperature observations from the fixed stations are all surface temperatures. Figure 5.2 shows a few outliers in the measurements at K13 and SON which have not been removed. Furthermore, the figure shows that the temperatures at K13 are generally higher and at SON generally lower and with higher daily variations.
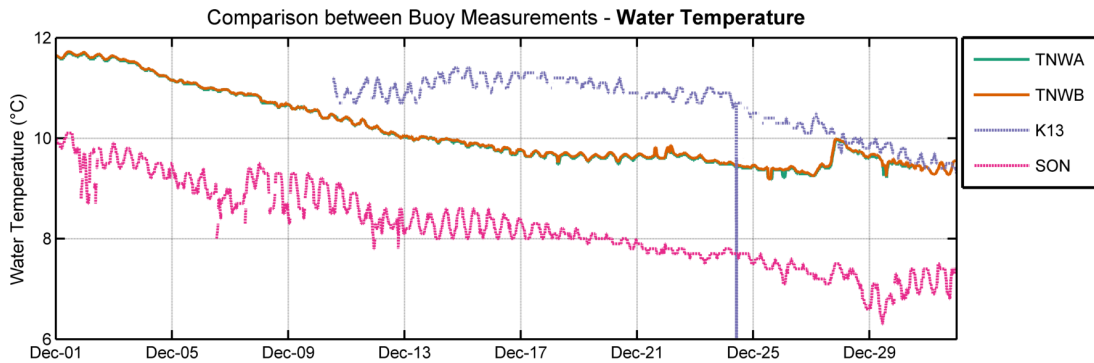

Figure 5.2: *Water temperature measurements from all locations (data from December 2020).*

A direct comparison of the measured surface water temperature at TNWA and TNWB against the fixed stations is provided in Figure 5.3 and Figure 5.4, respectively. As could already be inferred from the spatial variations shown in Figure 5.2, the agreement between the TNWA and TNWB temperatures and those at SON is good and those at K13 is poor.
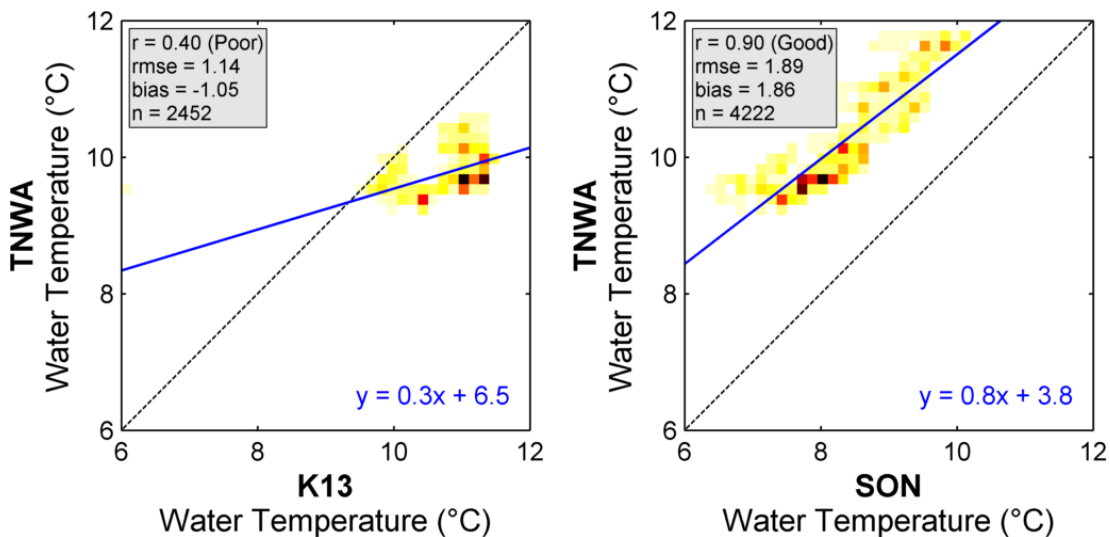

Figure 5.3: *Surface water temperature comparison at TNWA (data from December 2020).*
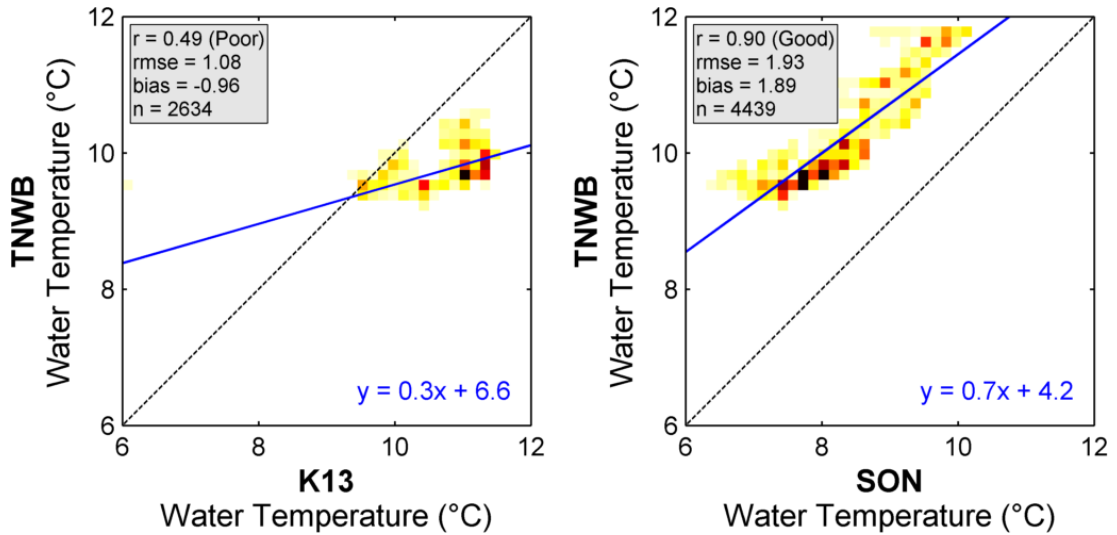
Figure 5.4: *Surface water temperature comparison at TNWB (data from December 2020).*

5.2.2 Air Temperature

A timeseries comparison of the measured air temperature between the observations at TNWA and TNWB and those at BG is provided in Figure 5.5. All datasets align with lower air temperatures at BG. A direct comparison of the measured air temperature at TNWA and TNWB and the observations at BG is provided in Figure 5.6. As could also be seen in Figure 5.5, the agreements are all excellent. Note that the stepwise timeseries of BG is due to the coarse (1 °C) discretization of the available raw measurements.
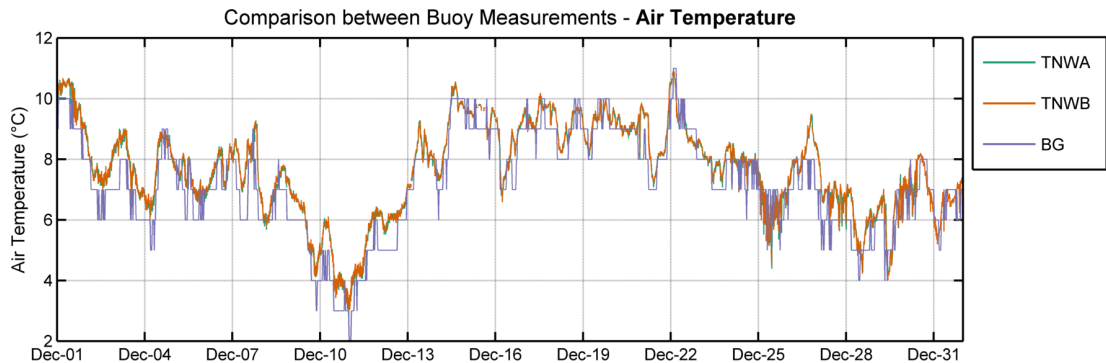
Figure 5.5: *Air temperature measurements from all locations (data from December 2020).*
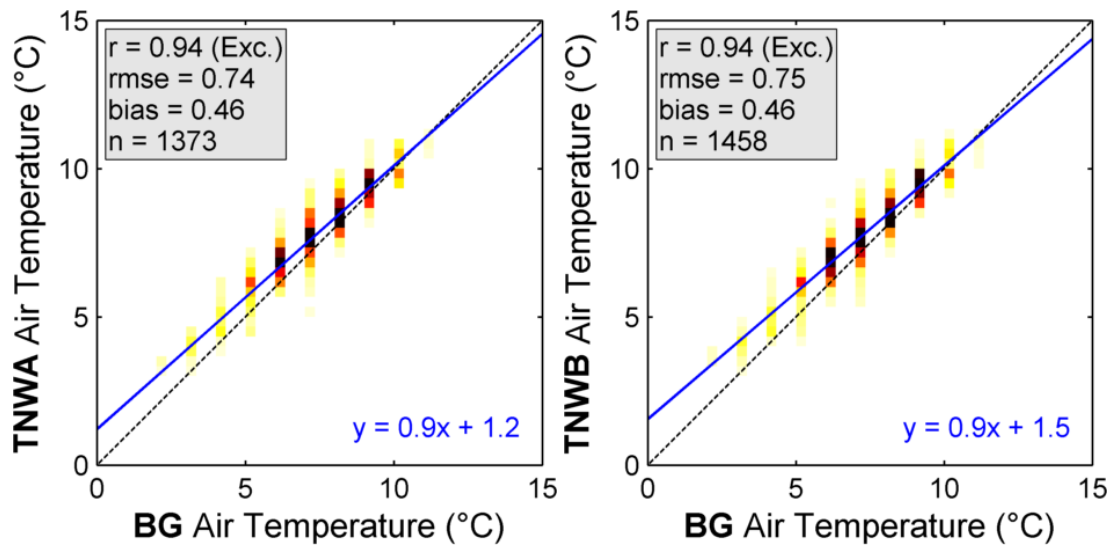
Figure 5.6: *Air temperature comparison at TNWA (left panel) and TNWB (right panel). Data from December 2020.*

5.3 Conclusions

The validation of the temperature data shows that there is an excellent agreement between TNW air temperature observations and those from the considered fixed station. Furthermore, due to spatial variations there are mismatches between TNW surface water temperature observations and those from the fixed stations.

6 Air Pressure

6.1 Overview

An overview of the available air pressure measurements from TNWA, TNWB, L91, K13, and F3 is shown in Figure 6.1. The signals show near-identical variations in time, as expected, given their proximity with respect to macro-atmospheric forcings. The figure also shows that there is most of the time an offset between the L91 data and the data from the other stations, which is not as expected and can be seen as an indication of biases in the L91 data.
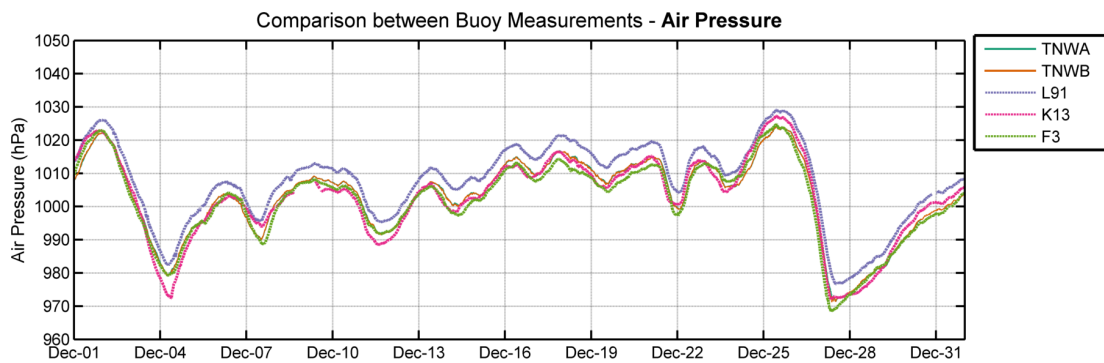
Figure 6.1: *Air pressure measurements from all locations.*

6.2 Validation

A direct comparison of the measured air pressure at TNWA (TNWB) against those of the fixed stations is given in Figure 6.2 (Figure 6.3). As could already be inferred from the variations shown in Figure 6.1, the agreements are all excellent and there is a bias of about 4 hPa between the L91 and the TNW data.
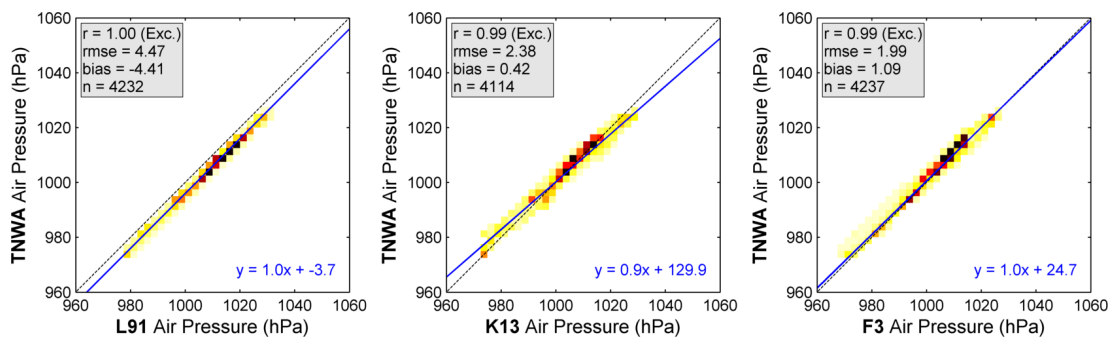
**Figure 6.2:** *Air pressure comparison at TNWA (data from December 2020).*
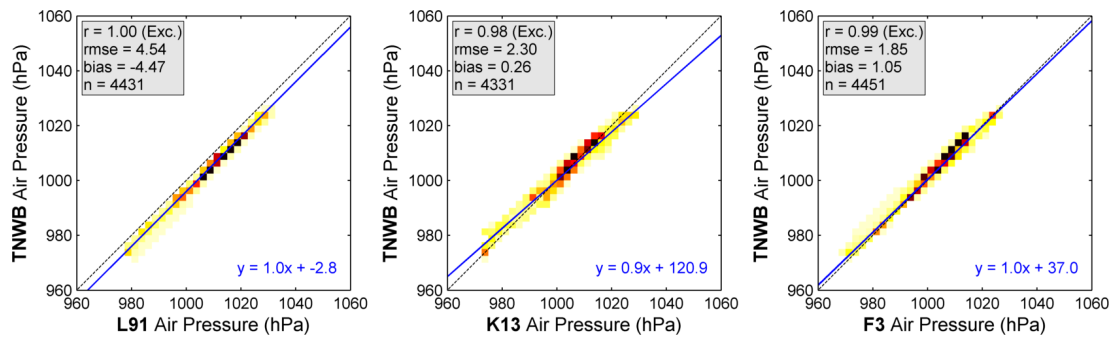
Figure 6.3: *Air pressure comparison at TNWB (data from December 2020).*

6.3 Conclusions

The validation of the air pressure data shows, as expected given their proximity in terms of macro-atmospheric forcings, an excellent agreement between the TNW observations and those from the fixed stations.

7 Currents

7.1 Ten Noorden van de Waddeneilanden description

During this period there are no currents observations available from TNWB. At TNWA the current speed and direction are available at depths 3 to 38 m with a spacing of 1 m. Even though the observations close to the bottom are of lower quality and not always available due to the water level variations, in this report we still consider the current velocity data down to a (near bottom) depth of 36 m.

To get a full overview of the data a movie was created with the time evolution of vertical current profiles at TNWA (see here). Furthermore, Figure 7.1 shows the timeseries of the observed surface (3 m) current speeds, with the corresponding rose being given in Figure 7.2, Figure 7.3 shows the observed current speeds and directions as a function of depth and Figure 7.4 shows all TNWA observed vertical current profiles (grey lines) and the mean profile (red line). As can be seen in the figures, the currents in TNW are predominantly tidally driven, with an alignment close to East-West and with the stronger currents being towards the East.
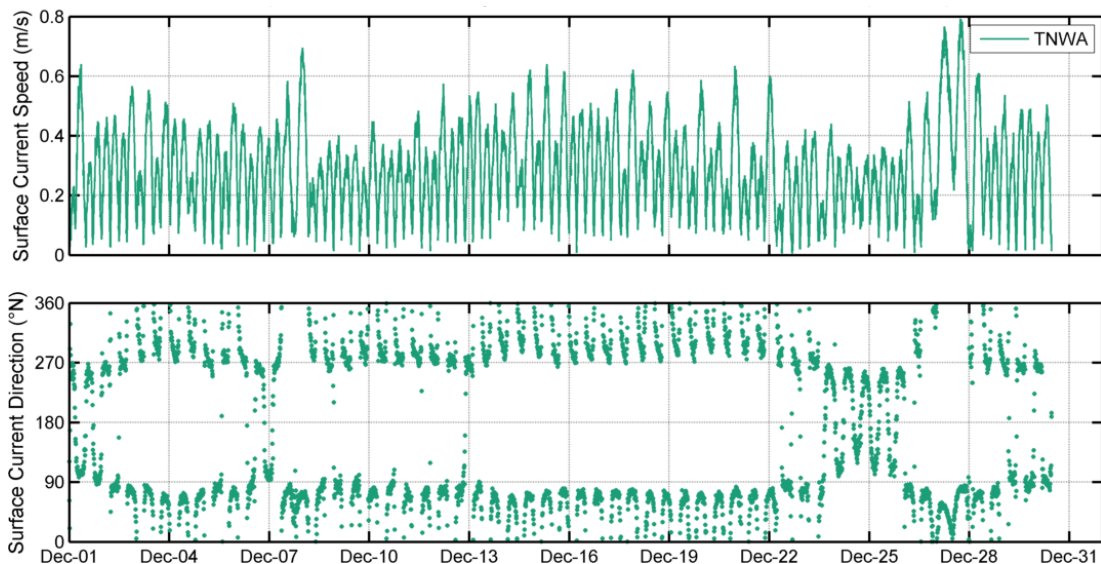
Figure 7.1: *TNWA surface current speed (top) and direction (bottom). The oceanographic convention is used for the current directions, so all current directions are going to, clockwise from North.*
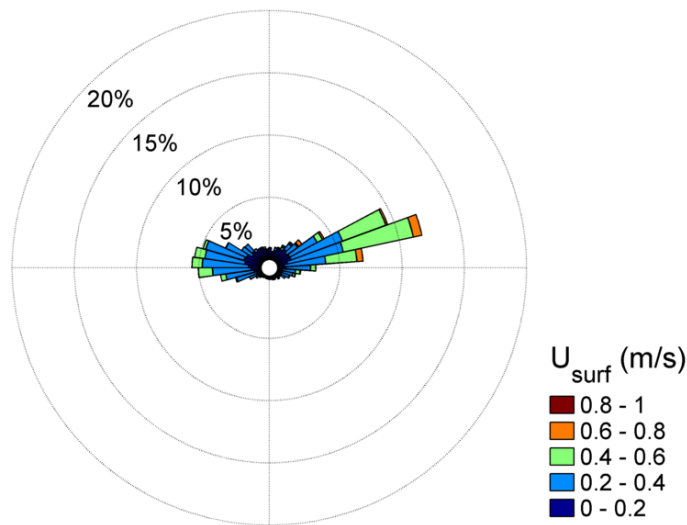
Figure 7.2: *TNWA surface (3 m) current rose (bin width 8°) (December 2020). The current direction is the direction the piles point to away from the centre of the rose.*
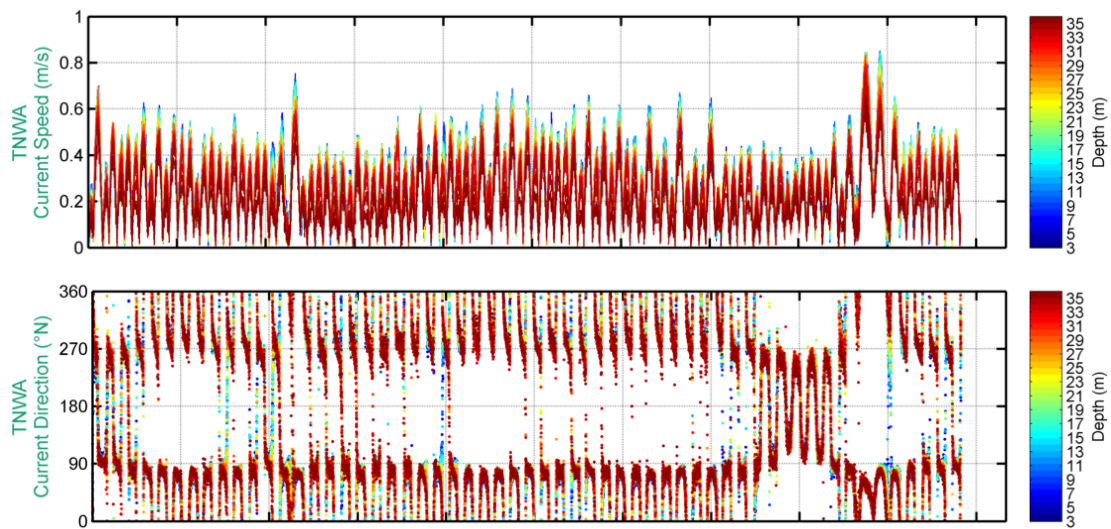

Figure 7.3: *TNWA current speeds (top) and directions (bottom) by depth (December 2020). The oceanographic convention is used for the current directions, so all current directions are going to clockwise from North.*
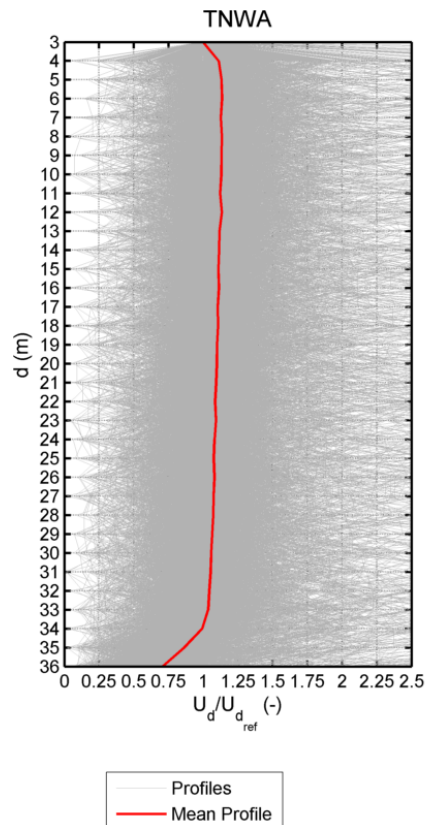
Figure 7.4: *Normalized (with relation to the 3 m level) TNWA current speed vertical profile (December 2020). The x-axis has a fixed lower limit of 0 and upper limit of 2.5 for readability.*

7.2 Validation

The validation of the measured currents is completed with data from Deltares 3D Dutch Continental Shelf Model-Flexible Mesh (3D DCSM-FM) described in Appendix A. Given the lack of 3D current data from other sources, 3D DCSM-FM has been run purposely for this validation.

A direct comparison between the 3D DCSM-FM surface current (d = 3 m) at TNWA and the buoy observations is given in Figure 7.5 in terms of timeseries and Figure 7.6 in terms of roses. The same comparisons are shown in Figure 7.7 in terms of timeseries and Figure 7.8 in terms of roses for the current at 23 m (about 60% down the water column). At the agreements are excellent in terms of current speed both levels and poor (23 m) to reasonable (3 m) in terms of current direction. Furthermore, the roses show more directional spreading in the observations and a larger west-east current asymmetry, with a higher predominance of currents towards the East in the observations.

As demonstrated in previous reports, the low current direction correlations can to a large extent be explained by the nature and variability of the current direction signal. Due to the rotating nature of the currents, especially when they rapidly rotate towards offshore (directions close to 350) the timing can be off. This affects mainly the buoy observations and occurs during short time periods and mostly when the current speeds are low.
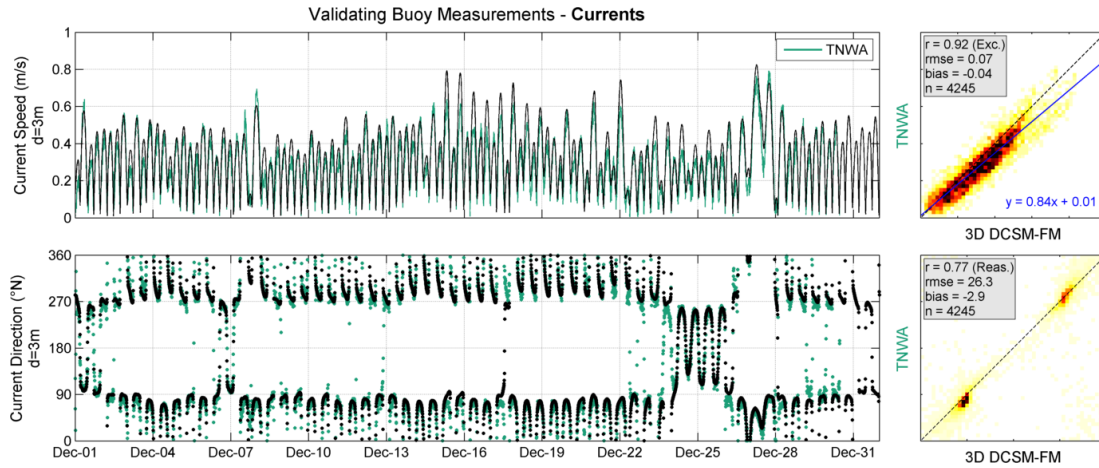
Figure 7.5: *Surface (d=3 m) current comparison at TNWA (data from December 2020).*

Figure 7.6: *Buoy and 3D DCSM-FM roses (bin width 8°) of the surface (3 m) current velocity at TNWA (data from December 2020. The current direction is the direction the piles point to away from the centre of the rose.*
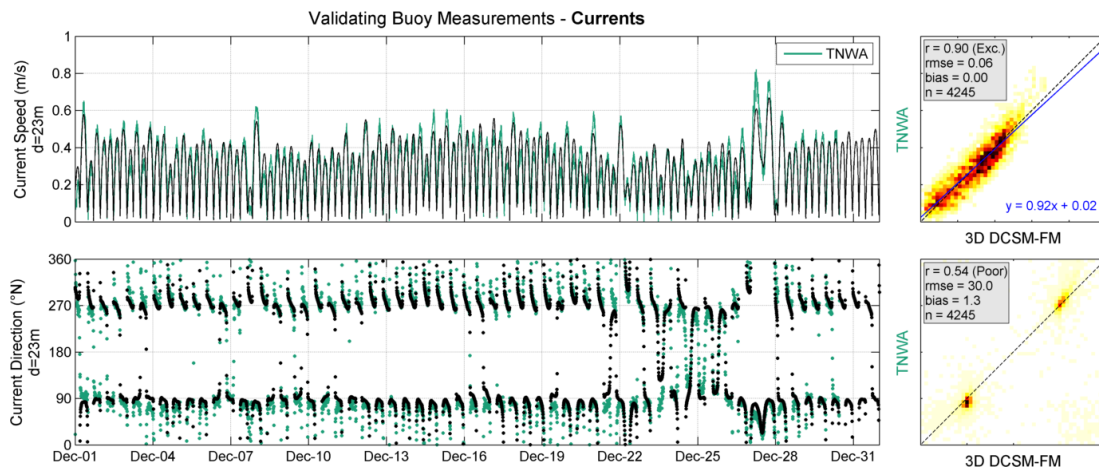

Figure 7.7: *Current comparison at depth of 23 m TNWA (data from December 2020.*

TNWA comparison between buoy and 3D DCSM-FM currents (d = 23 m)
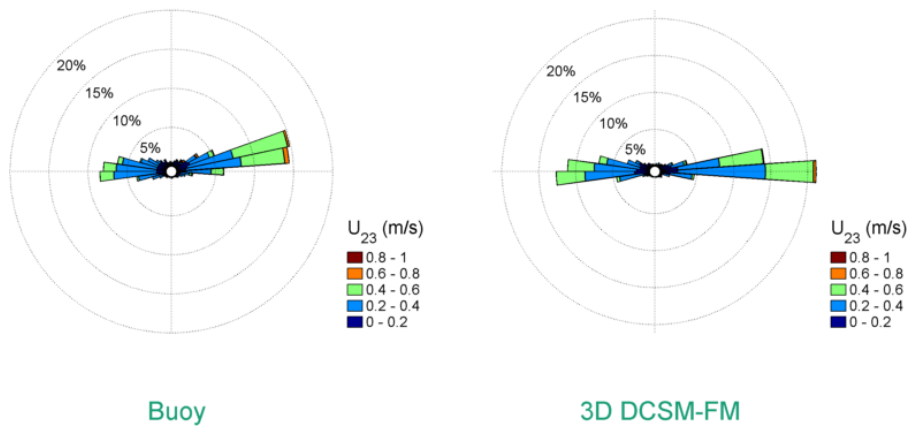
Figure 7.8: *Buoy and 3D DCSM-FM roses (bin width 8°) of the 23 m current velocity at TNWA (data from December 2020). The current direction is the direction the piles point to away from the centre of the rose.*

Table 7.1 shows the error statistics between the current speed and direction of the model at TNWA and the TNWA data at the observed levels from a depth of 3 m to 36 m. In terms of current speed the agreements are reasonable at the lower two levels and good to excellent from the 34 m level until the surface. In terms of current direction the agreements are poor to reasonable.

Table 7.1: *Statistical comparison between the 3D DCSM-FM results with TNWA with depth.*

Depth (m)	Current Speed				Current Direction		
	r (-)	Bias (m/s)	Symm. Slope (-)	n (-)	r (-)	Bias (°)	n (-)
3	0.92	-0.04	0.88	4245	0.77	-2.9	4245
4	0.92	-0.02	0.95	4245	0.79	-2.2	4245
5	0.92	-0.01	0.96	4245	0.79	-1.6	4245
6	0.92	-0.01	0.97	4245	0.76	-1.6	4245
7	0.92	-0.01	0.97	4245	0.76	-1.3	4245
8	0.92	-0.01	0.98	4245	0.73	-1.3	4245
9	0.92	-0.01	0.98	4245	0.74	-1.9	4245
10	0.92	-0.01	0.98	4245	0.71	-1.2	4245
11	0.92	-0.01	0.98	4245	0.72	-0.9	4245
12	0.92	-0.00	0.99	4244	0.68	-0.4	4244
13	0.92	-0.00	0.99	4245	0.69	-0.1	4245
14	0.92	-0.00	0.99	4245	0.66	0.1	4245
15	0.92	-0.00	0.99	4245	0.67	0.4	4245
16	0.92	-0.00	1.00	4245	0.62	0.4	4245
17	0.92	-0.00	1.00	4245	0.63	0.4	4245
18	0.92	-0.00	1.00	4245	0.59	0.3	4245
19	0.92	0.00	1.00	4245	0.58	0.7	4245
20	0.92	-0.00	1.00	4245	0.56	1.1	4245
21	0.91	0.00	1.01	4245	0.55	1.1	4245
22	0.91	-0.00	1.00	4245	0.55	1.0	4245
23	0.90	0.00	1.01	4245	0.54	1.3	4245
24	0.91	0.00	1.01	4245	0.53	1.3	4245
25	0.90	0.00	1.01	4244	0.53	1.1	4244
26	0.89	0.00	1.01	4245	0.53	1.7	4245
27	0.88	0.00	1.03	4245	0.52	1.8	4245
28	0.88	0.00	1.02	4245	0.51	1.3	4245
29	0.87	0.01	1.03	4245	0.48	1.8	4245
30	0.87	0.00	1.02	4245	0.49	1.1	4245
31	0.85	0.01	1.04	4245	0.49	1.9	4245
32	0.85	0.00	1.02	4245	0.49	1.3	4245
33	0.84	0.01	1.04	4245	0.49	1.8	4245
34	0.83	-0.00	1.00	4245	0.51	0.1	4245
35	0.78	-0.02	0.94	4245	0.51	0.7	4245
36	0.70	-0.06	0.79	4245	0.41	3.1	4245

7.3 Conclusions

As shown above, there is a high agreement between the current speed observations from TNWA and the model results. The obtained low correlations between the current directions are not considered to be due to lack of accuracy in the current direction observations, but model resolution effects and the effect of the nature and variability of the current direction signal on the buoy observations. The found general agreement between the buoy and model data, testify to the quality of both the model results and the observations.

References

DNV-GL, 2019. *FUGRO SEAWATCH WIND LIDAR BUOY WS 190 PRE-DEPLOYMENT VALIDATION; Assessment of the Fugro Seawatch Wind LiDAR Buoy WS 191 Pre-Deployment Validation at Frøya, Norway*. Tech. Rep. 10129033-R-11, Rev. A, 2019-06-25, DNV-GL.

EMODnet Bathymetry Consortium, 2016. *EMODnet Digital Bathymetry (DTM),* `http://doi.org/10.12770/c7b53704-999d-4721-b1a3-04ec60c87238`. Tech. rep.

Fisher, N. I., 1993. *Statistical analysis of circular data*. Cambridge Univ. Press.

Fisher, N. I. and A. J. Lee, 1983. "A correlation coefficient for circular data." *Biometrika* 70: 327–332.

IEA Wind, 2017. *"18. FLOATING LIDAR SYSTEMS", IEA Wind Expert group report on recommended practices, 1st edition, September 2017*. Tech. rep.

IEC 61400-12-1, 2017. *IEC 61400-12-1 Wind energy generation systems | Part 12-1: Power performance measurements of electricity producing wind turbines . IEC-TC88 Maintenance Team MT12-1 , Edition 2.0 , 3 March 2017*. Tech. rep.

KNMI, 2009. *HiRLAM version H7.2*. Tech. Rep. `http://projects.knmi.nl/datacentrum/catalogus/catalogus/content/history/HIRLAM72_eng__151009.pdf`, KNMI.

Wieringa, J. and P. Rijkoort, 1983. *Windklimaat van Nederland (in Dutch)*. KNMI (staatsuitgeverij).

Zijl, F. and J. Veenstra, 2018. *Setup and validation of 3D DCSM-FM*. Deltares memo 1220339-005-zks-0003.

Zijl, F., M. Verlaan and H. Gerritsen, 2013. "Improved water-level forecasting for the Northwest European Shelf and North Sea through direct modelling of tide, surge and non-linear interaction." *Ocean Dynamics* 63 (7).

A Hydrodynamic model

3D DCSM-FM covers the northwest European continental shelf, specifically the area between 15°W to 13°E and 43°N to 64°N, and includes the North Sea and adjacent shallow seas and estuaries such as the Wadden Sea and the Eastern and Western Scheldt. It is loosely based on the two-dimensional operational water level forecasting models of the Netherlands (Zijl *et al.* 2013), but uses a flexible mesh with resolution increasing with decreasing water depth (Figure A.1). The smallest cells have a size of 2/3' in east-west direction and 1/2' in north-south direction, which corresponds to 840 m by 930 m in Dutch waters. The optimization methodology is similar to (Zijl *et al.*, 2013), but excludes bathymetry adjustment. The bathymetry is based on a gridded bathymetric dataset (October 2016 version) from the European Marine Observation and Data Network (EMODnet; EMODnet Bathymetry Consortium, 2016) supplemented with survey data for the Dutch coastal zone (cf. Figure A.2)). 3D DCSM-FM uses 20 equidistant sigma-layer in the vertical and includes temperature and salinity as state parameters.
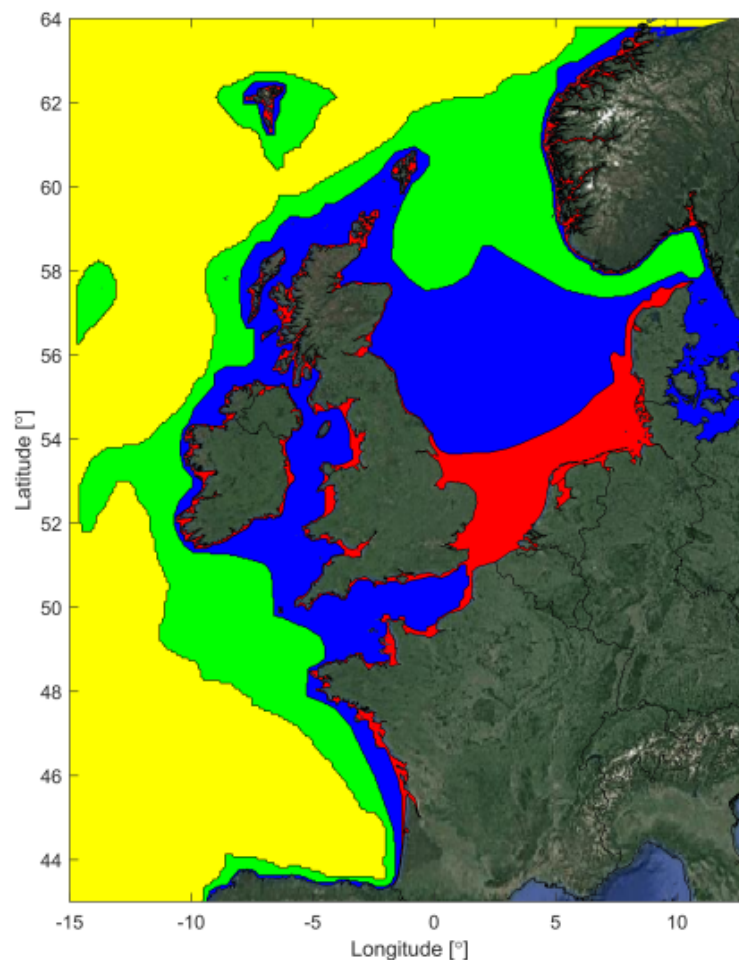

Figure A.1: *Overview of the 3D DCSM-FM model network with the colors indicating the grid size (yellow: ≈ 4 nm; green: ≈ 2 nm; blue: ≈ 1 nm; red: ≈ 0.5 nm).*
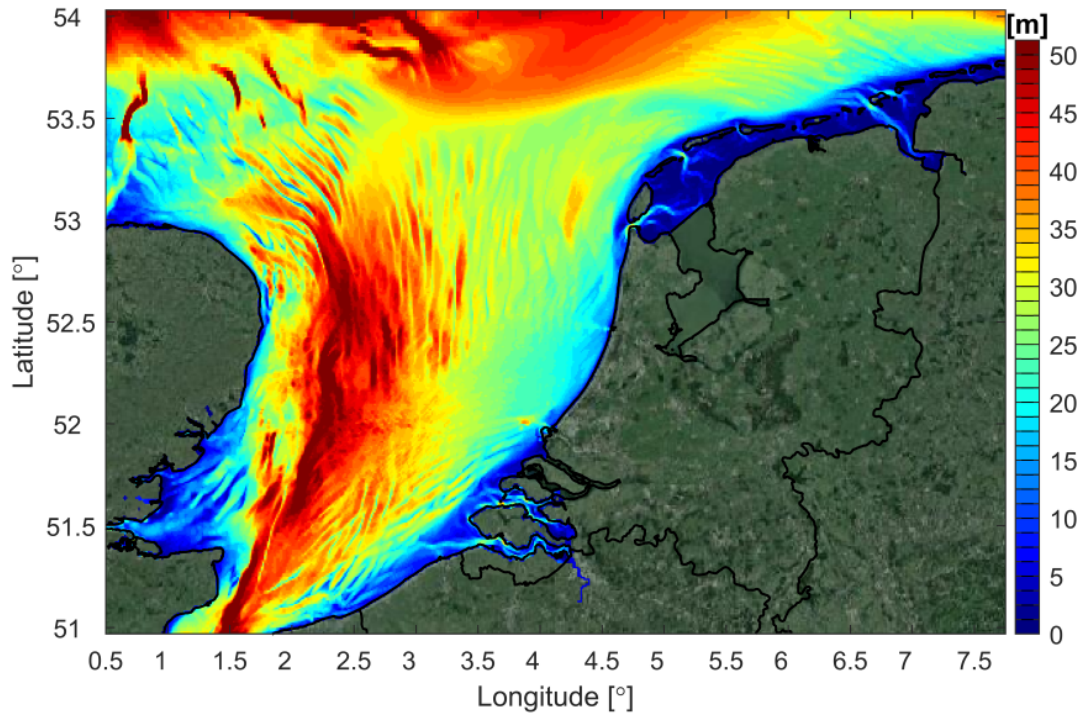
Figure A.2: *3D DCSM-FM model bathymetry in the southern North Sea (depths relative to MSL; source: EMODnet).*

At the lateral open boundaries water levels consisting of a tide and surge component are provided. For the tide 33 harmonic constituents from the global tide model FES2012[1] were used, while for the surge an Inverse Barometer Correction is applied (Zijl *et al.*, 2013). The model includes river discharges, while meteorological forcing in terms of atmospheric wind, mean level pressure, air temperature, cloud cover and dew point temperature are obtained from the KNMI operational Numerical Weather Prediction model Hirlam7.2. (Zijl and Veenstra, 2018) provides further details on the set-up and validation of 3D DCSM-FM .

---

[1]https://www.aviso.altimetry.fr/en/data/products/auxiliary-products/global-tide-fes/description-fes2012.html